NORTHWESTERN UNIVSERSITY

Inorganic Nanowells and Nanotubes as Templates for Chemical Nanofabrication

A DISSERTATION

SUBMITTED TO THE GRADUATE SCHOOL IN PARTIAL FULFILLMENT OF THE REQUIREMENTS

For the degree

DOCTOR OF PHILOSOPHY

Field of Chemistry

By

Jeremy Edward Barton

EVANSTON, ILLINOIS

June 2008

ABSTRACT

Inorganic Nanowells and Nanotubes as Templates for Chemical Nanofabrication

Jeremy Edward Barton

Nanoscale materials are demonstrating new properties and promising applications with each passing day. The fabrication of ever more complex and precise nanomaterials represents a continuing drive in the fields of physics, chemistry, and biology. Template-based approaches provide an attractive method of producing new inaccessible materials by modifying and confining older techniques, but most of the templates available today function only in a narrow range of chemical parameters. In this work, new thermally and chemically robust 'nanowell' templates were built to study confined precipitation as a method to fabricate nanomaterials. These templates consisted of two-dimensional arrays of 50 to 100-nm diameter (50-500 zL) hemispherical impressions in silicon and tantalum oxide. We found that after loading these nanowells by discontinuous dewetting the solvent rapidly evaporated, and the solute within each well crystallized into a single nanocrystal. The size of that nanocrystal depended on the size of the well and the concentration of the solution. We reduced metal salt precursor nanoparticles in a high temperature hydrogen atmosphere to fabricate metallic and metal oxide nanoparticles, and experiments were carried out to determine the nature and limits of nanoscale precipitation to generate novel nanomaterials. We found that in the presence of an existing nanoparticle, any new material loaded into the well would preferentially precipitate in contact with the existing nanoparticle. This phenomenon was applied to fabricate intermetallic nanocrystals.

To grow tantalum oxide nanowells, we studied the electrochemical self-ordering of anodized tantalum oxide into porous films and nanotubes. We found that in electrolytes of fluorine ions in concentrated sulfuric acid, tantalum films could be electrochemically oxidized into ordered porous structures whose spacing depended linearly on the applied voltage. The structural parameters of these porous films depended on the precise chemical composition of the electrolyte solution. Finally, we found that by annealing these oxide nanotubes under H_2S, they could be converted to superconducting tantalum disulfide inorganic fullerenes with a superconducting transition temperature 2 K higher than the bulk transition temperature (0.8 K).

Professor Teri W. Odom
Research Advisor

ACKNOWLEDGEMENTS

This work owes a great deal to the people around me. First and foremost, I would like to acknowledge Dr. Teri W. Odom, my advisor and PI, for her advice and support. This would not have been possible without her. I want to thank Prof. Chad Mirkin and Prof. Joe Hupp for serving as committee members and for providing constructive criticism over the past five years.

I want to acknowledge my friends Dr. Liza Babayan and Dr. Eric Greyson. We were the first of Teri's students, and setting up the lab together was a unique experience I wouldn't trade for anything. I treasure the stimulating scientific conversation, the collaborative learning environment, and the fascinating ideas we all shared. I want to thank Christopher Stender for contributing his invaluable solid-state crystallization and x-ray characterization expertise, and I want to thank my colleagues Dr. Perumal Sekar, Dr. Liying Wang, Dr. Doo Young Kim, Christina Sweeney, Warefta Hassan, and Min Hyung Lee, who each supplied a great deal of valuable experimental and scientific support over the last five years. Finally, I want to acknowledge my undergraduate students Laura Hughes, Samuel Nyok, Wil Sufentes, Jennifer Y. Wang, and Jeff Wille, for their excellent work investigating the dynamics of microscale crystallization in various material systems.

On a more personal note, I made several friends within the research group over the last several years; Liza and Eric were great friends to me, and more recently Chris Stender has been a haven of laid-back stability. I have also been lucky enough to make several good friends beyond the boundaries of my research lab. I want to thank Michael Mousorrafiti, Christopher Konek, and Neeraj Saraiya for the personal support and perspective of those who know the trials and tribulations of science and have some distance from the gory details. Along side my newer friends, I also want to thank my oldest friends. Though we have long gone our separate ways, the

reunions, visits, and random chats with friends of old have done much to keep me sane. I want to thank Eldon Cowgur, Aaron Wright, Abby Spears, Erik Gable, Kenna McKenzie-Young, Elizabeth Ottesen, Talea Townsend, Laura Harris, Ben Kaiser, and Andrew and Laurie Vick. You guys keep me centered. This brings me to my newest friend. Arielle Halpern has been a true boon, and probably the best thing to happen to me here at Northwestern.

I am blessed with an amazing family whose support has been priceless over these last several years – I wouldn't have made it through here without them. With all that they have been through, they still have the time and the effort to spare offering me care and support. I can't thank any of them enough, and simple words could never do justice to the love and gratitude I hold for them all. I'm particularly grateful to my new nieces Grace and Claire. Discovering life anew through the eyes and minds of my nieces brings the wonder of our world into full focus… and should motivate us all to ensure that they have a better life than we do.

LIST OF COMMON ABREVIATIONS

2D – two-dimensional

3D – three-dimensional

GA-XRD - glancing angle x-ray diffraction

HR-TEM - high resolution transmission electron microscopy

MIMIC – micro-contact molding in capillaries

PXRD - powder x-ray diffraction

SAED - selected area electron diffraction

SEM – scanning electron microscopy

TEM – transmission electron microscopy

XPS - x-ray photoelectron spectroscopy

XRD - x-ray diffraction

TABLE OF CONTENTS

LIST OF ILLUSTRATIONS

Chapter 1

Introduction

1.1 General Overview

Richard Feynman introduced the concept of nanotechnology on December 29th, 1959 in a now famous lecture entitled 'There's Plenty of Room at the Bottom.' Most of those who attended reputedly did so with apprehension, suspecting the talk would be describing all the wonderful things physicists could waste their degrees on. Instead, Feynman spoke of a new frontier in science, at a length scale between 1 and 100 nm. This scale is small for engineers, commonplace for biologists, and large for chemists. It was Feynman's contention that physics and engineering could develop the tools work on this scale, and so directly image and manipulate atoms and molecules. He saw the potential of such a technology, not only to solve current problems by direct imaging and manipulation, but to open entirely new fields of science by building materials on a scale dominated by quantum mechanics rather than bulk continuum phenomena. Things behave *differently* when they are small.

The invention of the scanning tunneling microscope (STM) began the first tentative steps toward the direct imaging and manipulation capabilities Feynman outlined in 1959, and in the last twenty years there has been steady progress toward widespread atomic imaging and manipulation.[1] In the meantime, chemists and engineers have already moved into the nanoscale, developing a multitude of new fabrication and synthetic techniques based on established technology. Nanoscience is taking advantage of those tools to investigate the emergent properties of small systems and using those systems to generate additional tools for nanotechnology. Of the many different nanotechnology methods for material synthesis, one of the most promising toolsets is template-based synthesis: taking advantage of one nanostructure to grow a wide range of other nanostructures.

Soft organic materials such as micelles, dendrimers, and photoresist nanowells have been used successfully to template nanomaterials growth by limiting the available reactant to masses small enough to form single nanoparticles.[2-8] The concept is elegant, but these soft organic materials can only grow a small subset of nanoparticle materials because of comparatively low thermal stability. Inorganic templates have higher thermal stability, but there are few such templates for making zero-dimensional nanocrystals.

In contrast, porous alumina widely used as a template to grow one-dimensional (1D) nanostructures because it enables mass production without using expensive lithographic tools such as electron beam lithography. Porous alumina films can be fabricated electrochemically through anodic oxidation of aluminum films over square inch areas and have nanoscale features ranging from 50-600 nm.[9-18] These membranes have been used to template structures ranging from ordered arrays of nanowires and nanotubes to magnetic nanodots for investigating high density data storage to multicomponent nanorods for biological bar coding.[19-22] Common deposition techniques used in porous alumina are electroplating, electroless plating, CVD deposition, atomic layer deposition, and solution impregnation.[11, 18, 23-25] All of these depositions replicate the existing 1D structure of the alumina pore, using porous alumina to grow a number of new nanomaterials impossible to achieve by other methods. Until Feynman’s proposal is fully realized, the most efficient way to increase the number of nanoscale scientific and technological building blocks is to generate new synthesis templates. Each new template has the potential to open entirely new classes of established chemistry and engineering to nanoscale application.

1.2 Goals and Organization

The goals of this thesis are to develop and characterize new templates and techniques to grow nanoparticles and nanostructures. Chapter 2 describes the generation of zL volume nanowells in silicon substrates, their application as templates to confine the precipitation of nanoparticle precursor materials, and the conversion of precursor nanoparticles to metal or metal oxide nanoparticles by hydrogen reduction. The chapter then goes on to discuss our application of arrays of metal nanoparticles to investigate the mechanism of water-assisted carbon nanotube growth. Chapter 3 describes our work on developing large area arrays of nanowells in self-ordered anodic tantalum oxide films. These films are applied to grow nanoparticles similar to those in chapter 2, and the control of the nanowell depth and radius of curvature is applied to identify key factors in making high density nanowells capable of confined precipitation. We go on to separate the thin weakly bound tantalum oxide film from the substrate and place it on a transmission electron microscopy (TEM) grid. This unique substrate allows us to examine nanoparticles in nanowells by TEM and investigate the precipitation of nanoparticles into wells already containing nanoparticles. Chapter 4 goes into more depth on the anodization work in chapter 3 and details our investigation into the rapid growth of anodized tantalum oxide nanotubes, drawing strong parallels with porous alumina and TiO_2 self-ordering anodization. Based on our experimental findings, we propose a general mechanism for the growth of self-ordering anodic porous metal oxides.

Chapter 2

Laser Assisted Nanowell Fabrication and Nanoparticle Growth in Silicon

2.1 Background

2.1.1 Crystallization in Nanoreactors

Nanoscale crystals can exhibit new chemical and physical properties when their sizes become smaller than a key physical dimension.[26, 27] High temperature (150-250 ^{o}C) solution synthesis is one of the most successful methods to achieve size and shape control of nanocrystalline materials by controlling nucleation and growth kinetics in the presence of selective surfactant molecules.[28, 29] Inhomogeneity in the injection of precursors, mixing of the reactants, and temperature gradients in the reaction flask, however, can contribute to dispersions in the size of nanoparticles. To control the chemical and thermal homogeneity, small volume reaction vessels, such as dendrimers and reverse micelles, provide an appealing alternative.[30-32] The sizes of the nanoparticles formed within these structures depend on either the number of ions that can be intercalated into the dendritic branches or the interior water content of the micelles. Drawbacks to growth in these soft structures, however, include the polycrystalline nature of materials because of the low-temperature reaction conditions and the organic template that coats the nanoparticles. Small volume (<μm^3) reactors, in which particles could be grown at high temperatures and subsequently removed, are potentially a useful approach for achieving size control of crystalline nanoparticles.

2.1.2 Fabricated Nanoreactors

Micro- and nanofabricated structures have been used previously to template and direct the growth of crystalline materials from solution.[33-38] Templates such as anodized alumina membranes can generate polycrystalline nanorods with critical dimensions that are determined by the pore size (40-500 nm); electrodeposition is used to generate the quasi-ordered arrays of nanorods, which can be removed by etching the membrane.[11, 18-21, 25, 39, 40] Microfluidic reaction systems have also been employed to synthesize micro- and nanocrystals. Glass microchannel reactors and silicon micromixers were fabricated to grow nanoparticles of CdSe and CdS with well-controlled sizes by changing the reaction temperature, the concentration of precursors, and the flow rates.[36, 37] The microsystem reactors were typically operated in a continuous flow mode to produce concentrations of nanoparticles comparable to large scale growth. In addition, microcrystals of calcite and apatite were precipitated at the interface of laminar flow streams within PDMS microchannels.[41]

Arrays of structures that can prepare arrays of microcrystals from solution include micron-scale patterns of self-assembled monolayers (SAMs) and wells in soft materials (PDMS and photoresist).[42-45] Discontinuous dewetting can be used to form liquid droplets of uniform size on the hydrophilic portions of patterned SAMs and within microwells.[35] After the evaporation of the solvent, simple inorganic salts and organic molecular crystals precipitated into ordered arrays. The sizes of the crystals depended on the area of the hydrophilic region or the volume of the well in addition to the concentration of the reactants. This technique for particle growth has been applied to nanocrystals by growing 30-nm NaCl crystals in 100-nm wells of photoresist,[8] however the material properties of the wells limited the types of nanomaterials that could be grown. For example, these organic substrates are not robust at high (>100 °C) temperatures and are not compatible with polar or organic solvents and materials. The challenges of soft materials can be overcome by using harder, inorganic materials such as silicon and silicon dioxide, which are inert to common solvents and can withstand temperatures up to 900 °C. The use of nanofabricated structures made from these materials enables the growth and assembly of nanocrystals potentially more interesting than inorganic salts and organic molecular crystals.

Thus growth of nanocrystals in hard templates has several advantages: (i) simple syntheses based on bulk reactions; (ii) flexible size control achieved using different concentrations of precursor materials; (iii) generation of isolated nanocrystals in ordered arrays; (iv) the possibility of reusable templates for future reactions; and (v) broad material compatibility.

2.2 Fabrication of Arrays of Nanowells

One straightforward method to fabricate 100-nm scale features in silicon or other inorganic materials is laser assisted direct imprint (LADI) lithography.[46] In this technique, a patterned hard transparent mold, typically quartz, is used to emboss a silicon (Si) surface by melting the surface with a high intensity laser pulse. The silicon remains molten for approximately 200 ns and has a very low viscosity (0.003 cm^2s^{-1}), which allows silicon to flow easily into the mold.[47] Additionally, similar to the properties of water, Si (*l*) has a higher phase density than Si (*s*), thus, as the material cools it expands into contact with the nanostructured quartz mold.[48] These two factors enable <1 nm replication of the quartz mold in the silicon substrate.

2.2.1 Nanosphere Mold Fabrication

By using LADI lithography with a hexagonal close packed (HCP) Stöber silica microsphere mold, we can generate hemispherical nanowells in silicon substrates and apply these substrates to grow a diverse array of nanomaterials (Fig. 2.1). For imprint lithography to reproduce an accurate replica of the mold, the mold must be in direct contact with the substrate and under a uniform pressure.[46] Thus, care must be taken in the preparation of the mold. Standard drop coating methods yield domains with varying number of layers across the substrate.[49] This inhomogenaity prevents the establishment of uniform pressure across the substrate (Fig. 2.2). We devised three simple criteria for nanosphere mold fabrication. First, spheres must be highly

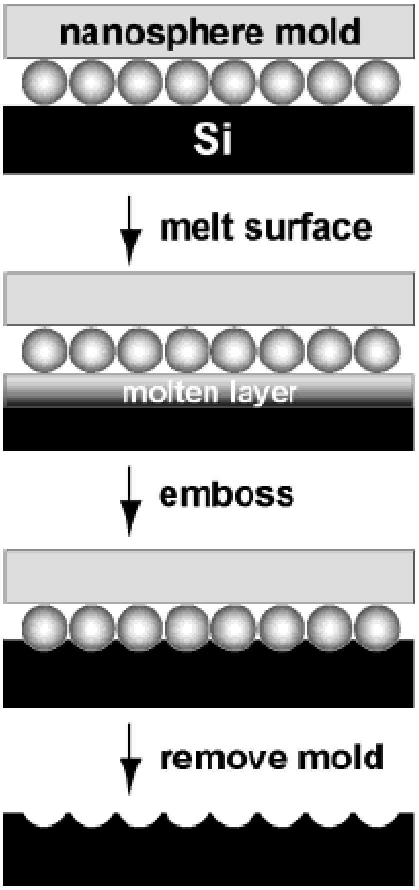

Figure 2.1: Scheme for fabricating nanoscale wells in silicon by laser-assisted embossing.

uniform in size. After approximately six months, we found that the surface of the silica spheres begin to roughen. Second, the mold must be in direct contact with the silicon surface. Rather than constructing a uniform reusable silica sphere mold on a piece of quartz, casting silica spheres directly onto the silicon surface achieves such contact most efficiently. Third, uniform pressure must be applied across the silica sphere mold to ensure the fabrication of nanowells. In areas where no pressure is applied, no nanowells will emboss, while areas with too much pressure yield thin layers of inverse opal as the molten silicon infiltrates through more than one sphere layer. In order to fabricate uniform nanowells across large areas, the mold must be flat.

In our work, a flat window was compressed against the coated substrate. This rigid mold only came into contact with the thickest portion of the sphere mold; thus a wide area of uniform height was required to achieve large embossing areas. If only a small portion of the sample was in contact with the compression plate, the embossing occurred over only an equally small area, and the applied pressure had to be reduced to prevent over-embossing. This problem was most prominent when aggregates in the sphere solution nucleate the growth of micron scale aggregates on the substrate; these aggregates rose above the surrounding spheres and came into contact with the window, embossing the substrate in disordered micron scale patches. In the presence of a uniform thickness of spheres, experiments with monolayers and multilayers revealed no difference in the results. Most experiments were carried out with multilayer silica sphere molds. All molds were cast on 3” silicon wafers, and then uniform areas were diced to fit the embossing cell.

100-nm diameter silica spheres were produced using a modified Stöber synthesis technique.[50] Briefly, an ethanolic solution of tetraethylorthosilicate (TEOS) was mixed with an ethanolic solution of ammonium hydroxide (NH_3OH) and water and stirred at room temperature for 1-12

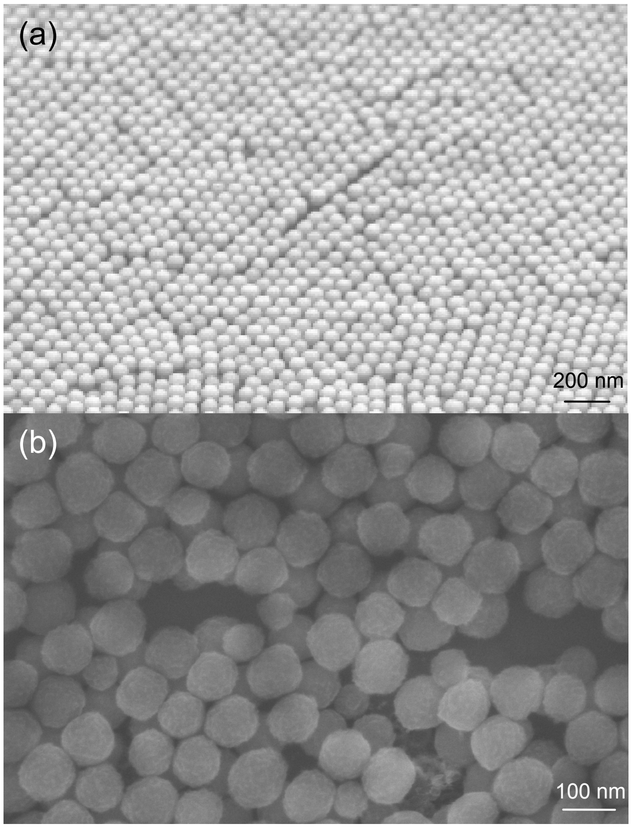

Figure 2.2: SEM images of (a) high quality multilayer silica sphere molds, and (b) typical low quality contaminated silica sphere molds.

hours. The size of the resulting microspheres depended on the concentrations of TEOS, water, and ammonia. The following empirical equations were used to determine the appropriate concentrations achieve the appropriate diameter (*d*) of the resulting spheres:[51]

$$d= A[H_20]\ 2\ \exp(-B[H_2O]^{1/2})$$

where

$$A = [TEOS]^{1/2}(82 - 151[NH_3] + 1200[NH_3]^2 - 366[NH_3]^3)$$

and

$$B = 1.05 + 0.523[NH_3] - 0.128[NH_3]^2$$

Prior to silica sphere deposition, silicon wafers were cleaned in a piranha bath (4:1 H_2SO_4:H_2O_2) at 70 °C to remove residual organic material, followed by a brief etch in 10% hydrofluoric acid (HF) to strip the native oxide. Substrates were then hydroxylated by a 10-s oxygen plasma etch in a PDC-32G 100 W plasma sterilizer under 2000 mTorr air to render the wafer hydrophilic. All silica sphere suspensions were filtered through a 450-nm pore diameter syringe filter in order to remove particle aggregates, and all substrates were dried over-night in a covered Petri dish.

Silica spheres were deposited on the silicon substrate either by drop-coating or convective self-assembly.[49, 52] In drop coating, the solid-liquid contact line is commonly pinned at the edge of the substrate, and as the suspension evaporates the height profile should reduce at all points causing the droplet to shrink. Since the contact line is pinned the droplet cannot shrink. To prevent shrinkage, solvent must flow toward the contact line,[49] and this outward flow of material draws a majority of the spheres in suspension to the edges of the wafer in the ‘coffee-stain’ effect.[53] By optimizing substrate size and shape, sphere concentration, solution volume, and evaporation rate, a portion of the substrate can be coated with a single monolayer of spheres as in colloidal lithography.[49]

Optimized drop-coating conditions for forming sphere monolayers on silicon wafers were found using a 1% w/w concentration of sphere solution. The monolayer consisted of a ~2 mm wide ring approximately 2 cm from the center of the substrate. This ring was adjacent to a disordered multilayer to the outside of the wafer and a disordered submonolayer region in the middle. Multilayer substrates were fabricated by drop-coating 500-μL of 5% by weight silica spheres across the silicon wafer. After drying, this procedure produced wafers with mm-scale grains of uniform height silica multilayers, suitable for use as small embossing molds. In order to increase embossing area, a modified convective self-assembly technique was introduced.

In convective self-assembly a hydrophilic substrate is placed at an angle between 9-90^{o} in a reservoir of colloidal suspension which is allowed to evaporate. This process establishes a low contact angle evaporation front on the hydrophilic substrate. Spheres are drawn into this contact line because of mass flow similar to that used in drop coating. Here spheres are forced into ordered multilayers, the thickness of which depends on the contact angle, the sphere concentration in solution, and the evaporation rate. In contrast to drop-coating, in convective self-assembly the spheres are deposited from a reservoir of slowly increasing concentration, thus the substrate is covered in a slowly increasing number of layers.[54]

The convective self-assembly technique was similar to the drop coating method described above, but the mechanism of the deposition differed. A silicon wafer was rendered hydrophilic with oxygen plasma, and coated with 500-μL of filtered solution of 5% w/w silica spheres. It was then placed in a covered Petri dish, inclined at a 9^{o} angle, and left to dry over a 12 h period. The convective self-assembly occurred at the top edge of the substrate, while the sphere reservoir was established at the bottom. This simple modification to the drying process resulted in cm-scale areas of uniform thickness, and allowed embossing of cm^2 areas.

Molds could also be patterned with micron scale structure by modifying the micromolding in capillaries (MIMIC) technique.[55] A poly-(dimethylsiloxane) (PDMS) pattern of 3-µm lines spaced by 3 µm was prepared by photolithography[8, 56] and placed in contact with an oxygen plasma treated silicon substrate. A droplet of solution was placed at an open end of the line pattern and the solution filled the lines by capillary action. After the solution dried and the PDMS mask was removed, the resulting sphere mold was several layers thicker within the patterned portions of the PDMS mold. These raised areas then act as the mold for embossing.

2.2.2 Laser Assisted Embossing Using Nanosphere Mold

Both drop-coating and convective self-assembly techniques formed well-ordered, close-packed layers at the surface of the silicon. A fused silica flat was then placed against the spheres, and a slight mechanical pressure was applied between the mold and the silicon substrate. The most effective compression cell consisted of three fused silica windows (1 cm x 1 cm x 1 mm) layered on top of each other, the sphere coated silicon substrate, and a 1 cm x 1 cm piece of steel. The substrates were compressed, by a screw in the cell, until the silica spheres were flush against the window across as much of the surface as possible (Fig. 2.3). Contact between the spheres and the window was estimated by observing the color change of the substrate. When the interference effect disappeared and the sample appeared brown, the substrate was considered to be in good contact.

A single 20-ns pulse from a KrF excimer laser (248 nm) was directed through the window with an energy density of 0.5-2 J cm^{-2}. This pulse melted the top surface (~20-200 nm) of the silicon substrate.[20] After the molten silicon cooled, and the silica spheres were removed by

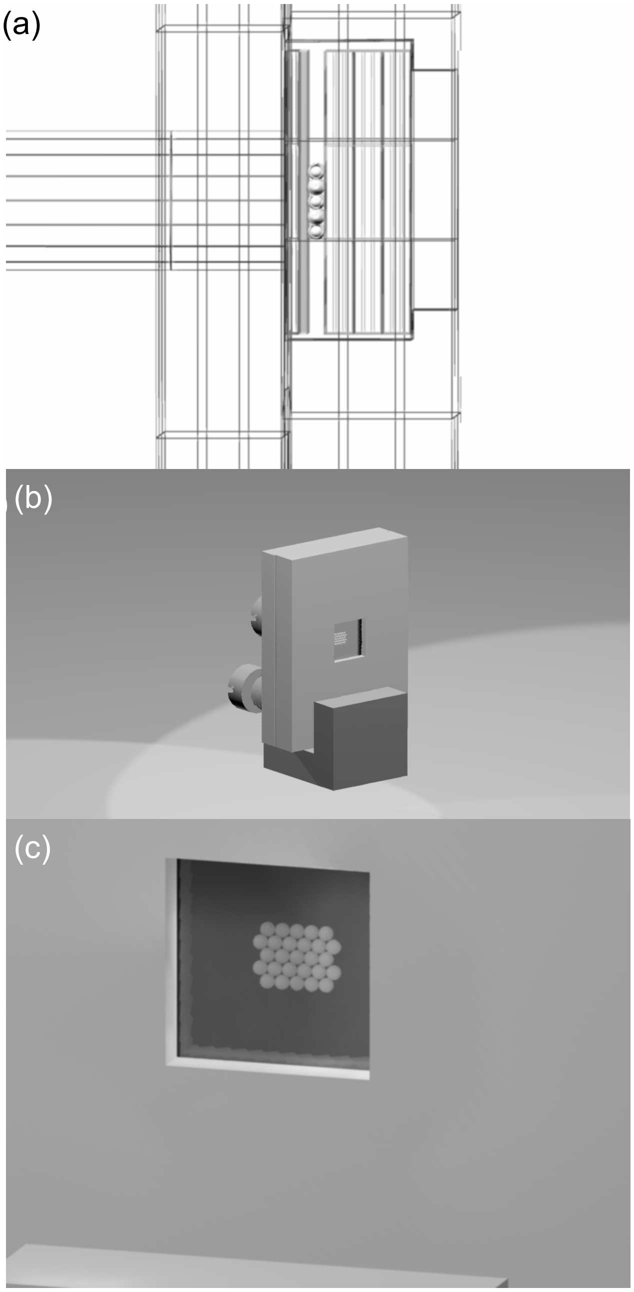

Figure 2.3: Diagrams and renders of (a) the compression cell in a wire frame diagram in, clearly displaying the three fused silica windows layered for mechanical strength, (b) a distant view of the compression cell, and (c) a close up view of a sphere coated substrate in contact with the windows.

etching in HF, the surface was embossed into nanowells. In areas of poor contact, the silicon flowed across the surface and solidified in a random morphology. This method proved amenable to a step-and-repeat process to increase the area of the embossed surface. Applying additional laser pulses to different areas of the substrate was a straight-forward means of increasing nanowell yield. Each pulse yielded ~2 mm^2 after embossing.

Figure 2.4 shows the successfully patterned silicon surface. The sizes of the nanowells were controlled by several factors: (i) the size of the spheres in the mold, (ii) the energy density of the laser pulse, and (iii) the applied mechanical pressure. The widths and separation of the nanowells were primarily determined by the physical size of the silica spheres, while the depth was affected primarily by the energy density (Fig. 2.4(c)).

The chemical composition of the nanowells was modified by thermal oxidation and by the growth of organosilane adlayers (octadecytricholorsilane and 1,1,2,2 tetrahydro(perfluorooctadecyl)trichlorosilane). Thermal oxidation of the patterned silicon substrates at 1000 ^{o}C for 7 h resulted in a size reduction in the wells of 10-20 nm in diameter (Fig. 2.4(d)), which may be attributed to the larger volume (~2 times) occupied by amorphous silicon dioxide compared to silicon.[57]

2.3 Nanoparticle Growth in Si Nanowells

In the absence of a chemical reaction, bulk crystallization occurs when two conditions are met: (i) the quantity of material dissolved in solution exceeds the carrying capacity of the solvent, and (ii) a nucleation point exists from which the solute can begin the crystallization process. The first condition can be reached by reducing the volume of the solvent by evaporation, cooling a

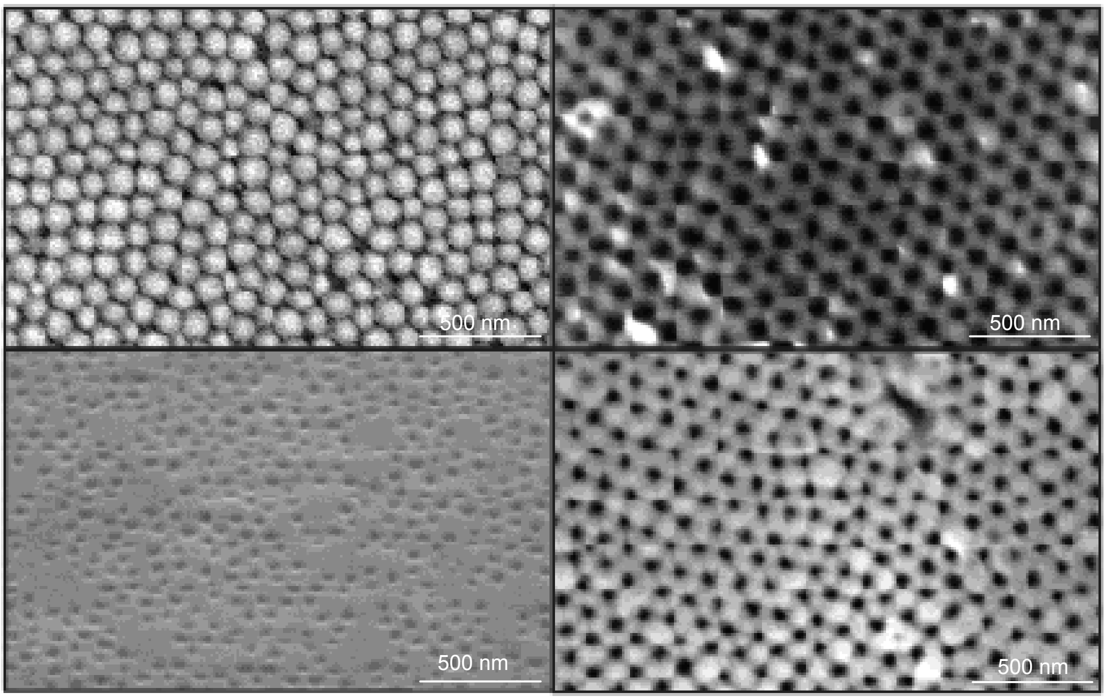

Figure 2.4: Scanning electron microscopy (SEM) image of (a) slightly disordered monolayer of 100 nm silica spheres. The disorder results from the polydispersity in sphere sizes. (b) Embossed nanowells. (c) Shallow nanowells embossed under low laser energy densities (0.8 J/cm^2). (d) Nanowells from (b) that were thermally oxidized. The diameters of the wells were reduced by 10-20 nm by oxidation.

saturated solution, or changing the composition of the solvent. The second condition occurs as crystals form in supersaturated solution or through the introduction of external nucleation points.

By using nanowells as crystallization dishes, we discovered that in the absence of external nucleation points, a single nanocrystal of solute was formed in each nanowell. Silicon nanowell substrates were loaded by discontinuous dewetting, specifically by withdrawing a patterned substrate perpendicularly from a solution at a rate between 2-100 μm/s.[35] In this way, each nanowell was filled with a similar quantity of solution (±5%)[35]; thus, varying the concentration of the solution allowed us to vary nanocrystal size from sub-1-nm diameters to a maximum diameter determined by the precursor solubility and the concentration of solution.[58]

2.3.1 Inorganic Salt Nanocrystals

We examined the effect of precursor concentration on nanoparticle diameter by crystallizing different concentrations of NaCl in similarly sized nanowells.[58] The nanowells were filled in a single step by discontinuous dewetting at 25 μm/s.[35] After the water evaporated, the precipitates in the wells were recrystallized in a humid atmosphere under short (2 s) exposure times.[18] Nanowells filled with 1 M salt concentrations resulted in smaller crystals than those formed from 5 M solutions. Square crystals of NaCl grown in 100-nm wells from a 1 M solution had edge lengths as small as 25 nm (Fig. 2.6). Because the SEM images were acquired with a tilt angle of 30°, nanocrystals pinned to the edges of the nanowells that face away from the detector were not visible.

2.3.2 Semiconducting Nanoparticles

In addition to the precipitation of simple inorganic salts, we used our nanowells to grow functional nanoscale materials. We created nanowells with hydrophobic surfaces for the preparation of CdS nanocrystals. The CdS reactions required two separate steps: (i) filling the

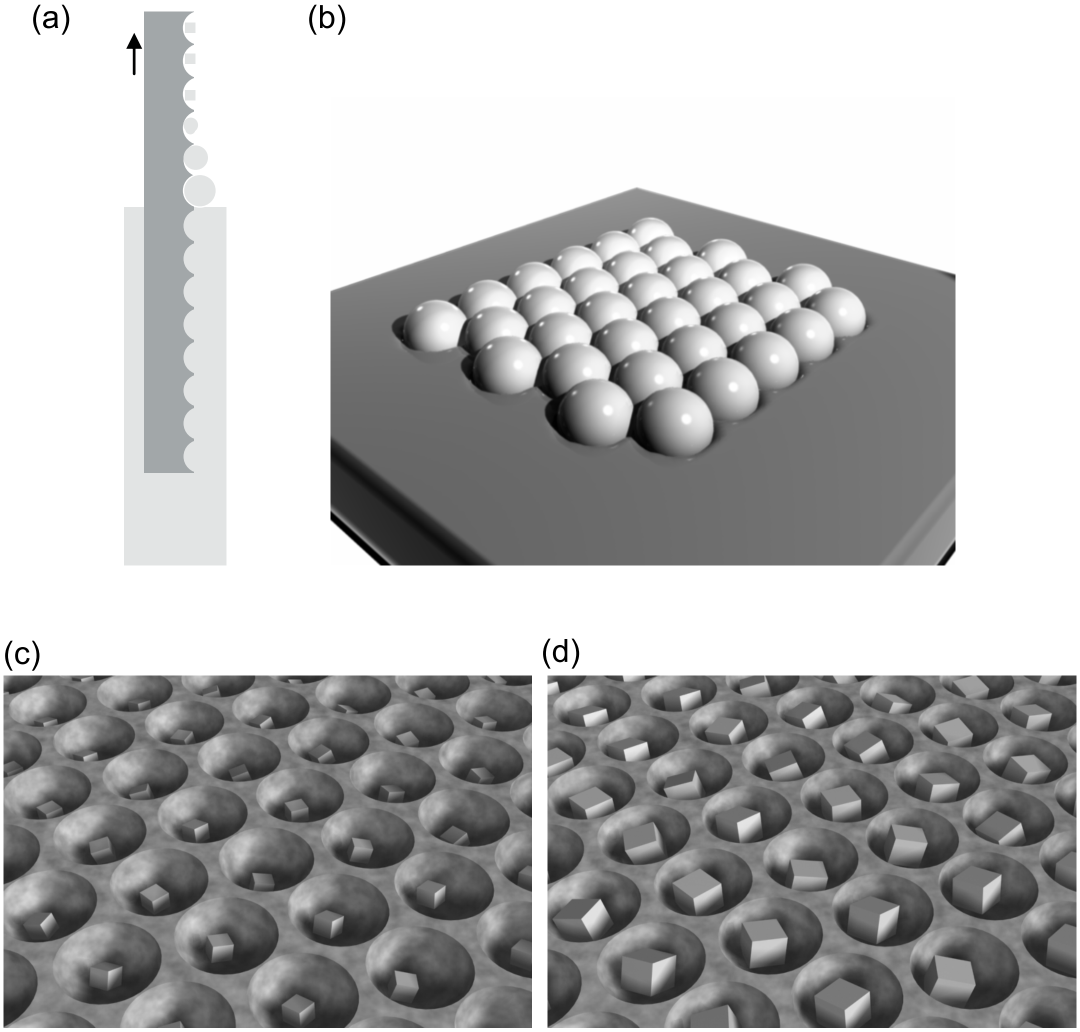

Figure 2.5: (a) A diagram of discontinuous dewetting and cartoons of (b) solution filled nanowells, (c) small crystals in nanowells from dilute solution, and (d) larger crystals in nanowells from concentrated solution.

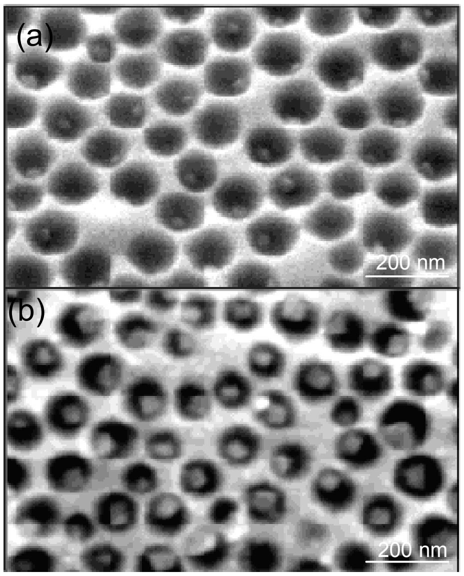

Figure 2.6: SEM images of individual NaCl nanocrystals grown within (a) 80 nm wells from a 1 M NaCl solution (tilt angle = 30°) and (b) 50-80-nm wells from a 5 M NaCl solution (tilt angle) 0°). The differences among nanocrystal sizes in (b) can be attributed to differences in well volumes and the local surface structure, which affect the amount of solution deposited within each well during the dewetting process.

wells

with cadmium acetate (0.1 M) by discontinuous dewetting (25 μm/s), and (ii) immersing the substrate into a sodium sulfide solution (1 M) for 5-10 s. Following step (i), single cadmium acetate nanocrystals remained in the nanowells; during step (ii), the cadmium acetate reacted with the sodium sulfide solution. The sample was washed with water to remove any unreacted precursor materials.

Figure 2.7 shows embossed nanowells in which CdS nanoparticles were grown. Higher resolution images revealed that each nanowell contained only one nanoparticle. To characterize crystallinity of the CdS, we removed the nanoparticles from the wells by sonication in hexane and analyzed them by TEM. The top inset of Figure 2.7 indicates that the small (~5 nm) CdS nanoparticles are crystalline; the lattice fringes correspond to (111) planes of CdS and are separated by 3.36 Å. We also annealed isolated CdS nanoparticles under Ar at 500 ^{o}C for 4 h to assist in the crystallization process; in general, the room temperature reaction conditions resulted in crystalline CdS nanoparticles. This simple, two-step process for synthesizing nanoparticles can form arrays of crystals simultaneously over areas up to mm^2.

This solution method has been used to grow crystalline CdS, but the number of available reactions which can be performed in this fashion is limited. The use of water soluble reactants for both precursor nanocrystal formation and chemical reduction restricts the available set of materials to reactions where the precursor does not have time to dissolve and diffuse out of the wells before reacting. To avoid this diffusion we have used high temperature hydrogen reduction to generate stable metal and metal-oxide nanoparticles.

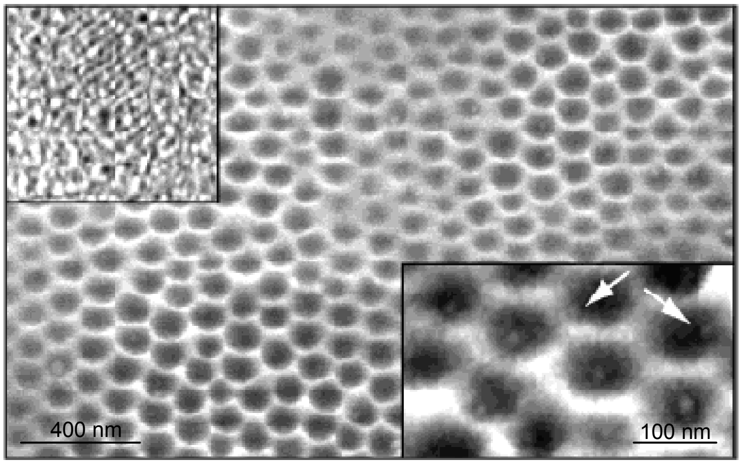

Figure 2.7: SEM image of an array of nanoscale wells that contain one CdS nanocrystal per well. The lower inset magnifies a small area of the array; the white arrows indicate crystals formed at the edges of the wells. The upper inset is a TEM image of an individual CdS nanocrystal removed from the array of nanowells by sonication. The separation between lattice fringes is 3.36 Å and matches the (111) plane of CdS.

2.3.3 Metal and Metal-Oxide Nanoparticles

In general, metal salt precursors can be loaded into nanowells and subjected to hydrogen reduction at temperatures ~80-90% of the precursor melting temperature. By this procedure, we were able to grow various metal and metal oxide nanoparticles with controlled sizes. The choice of solution chemistry was critical for this technique; to avoid non-specific binding the surface chemistry of the substrate must not react with the solvent or the metal salt precursors. Because most metal salts will physisorb to silicon dioxide, a high quality alkylsilane self-assembled monolayer was used to meet this surface-chemistry requirement, and we typically used substrates subjected to a twelve hour vapor deposition of octadecyltrichlorosilane on oxygen plasma hydroxylated substrates. The surface chemistry of these substrates was not stable under atmosphere for more than a day, and thus the substrates were either used immediately or stored under house vacuum for up to a week.

Gold nanoparticles were grown from a dimethlyformamide solution of chloro(triphenylphosphine) gold(I) precursor. Substrates were dewetted from this solution (50 μm/s) and subjected to hydrogen reduction in a 1” tube furnace at 400 ^{o}C. Substrates were held at this temperature for one hour and then oven cooled back to room temperature.

Iron and nickel oxide nanoparticles were grown from an aqueous solution of iron(III) chloride or nickel(II) chloride. Alkylsilanized substrates were dewetted at 50 μm/s and subjected to hydrogen reduction. Because the chloride precursors were more stable than the gold precursor, higher temperatures were used during the reduction process. Substrates were heated to 600 ^{o}C at a rate of 10 ^{o}C/s and then held at that temperature for 1 h before oven cooling to room temperature and imaging in the SEM. X-ray photoelectron spectroscopy (XPS) data revealed the Fe_2O_3 stoichiometry of the iron nanoparticles due to atmospheric oxidation.

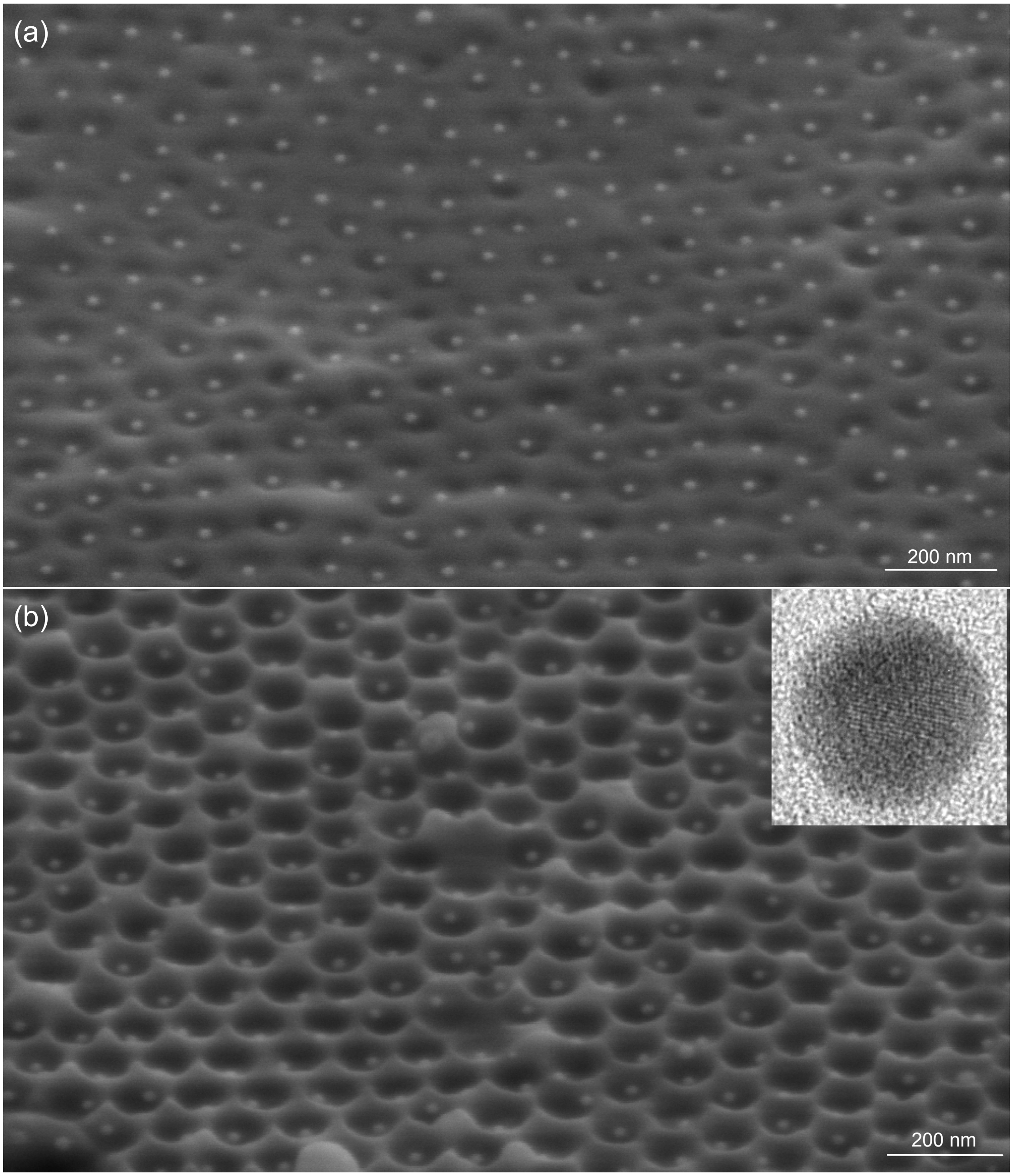

Figure 2.8: SEM images of Au nanoparticle grown in (a) shallow nanowells and (b) deep nanowells. The similar size distribution is due to the establishment of solvent droplets defined by the nanowell curvature, rather than by the absolute volume of the indentation. (b, inset) An HR-TEM image of an Au nanoparticle grown by this method.

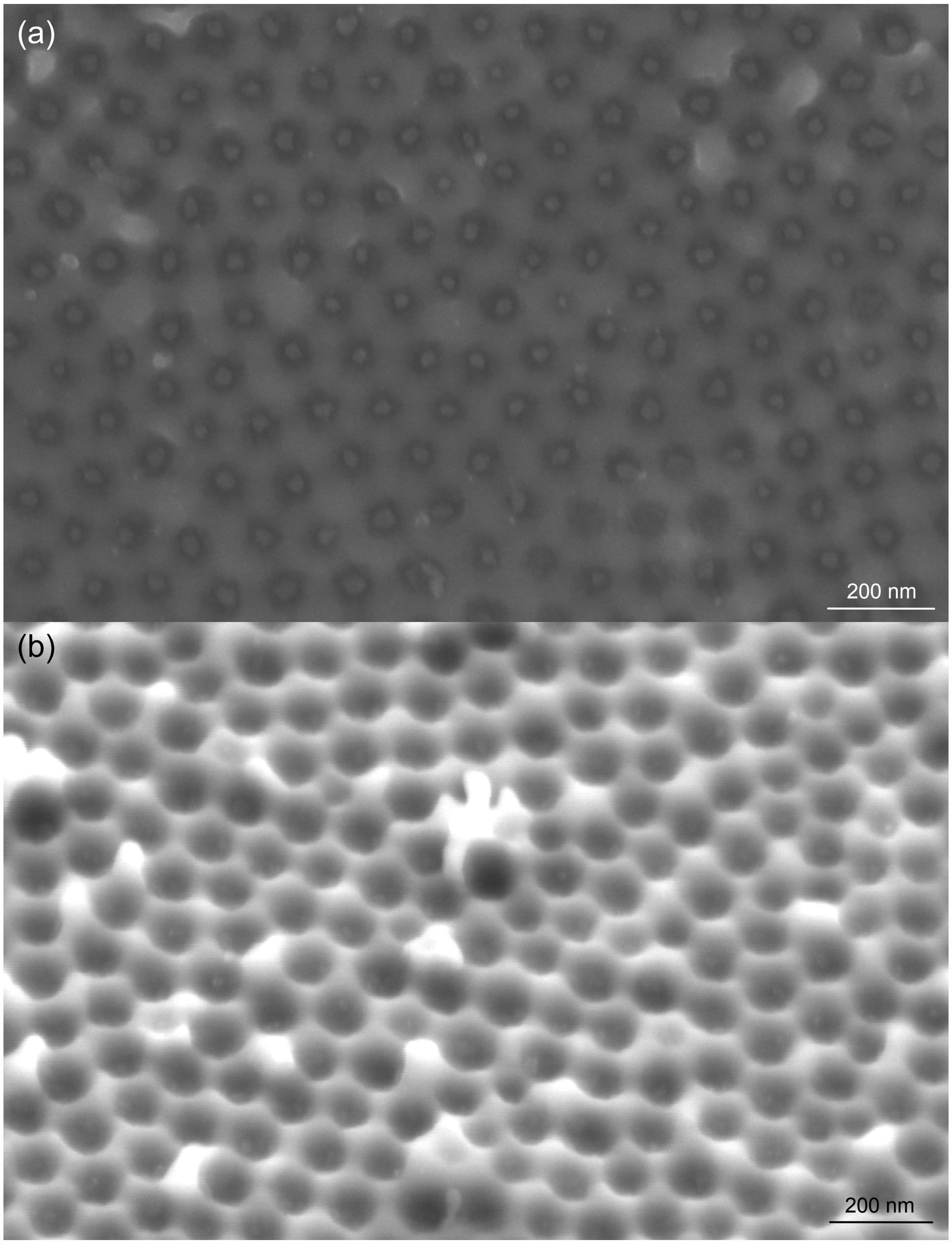

Figure 2.9: SEM images of (a) large nickel(III) oxide and (b) small iron(III) oxide nanoparticles.

2.3.4 Carbon Nanotube Growth

Metal and metal oxide nanoparticles are commonly used as catalytic particles for the growth of one-dimensional nanostructures.[27, 39, 59-61] For carbon nanotubes, the catalytic efficiency and ultimate result of these growth processes have been found to depend in part on the spacing and size of the catalyst particles.[62, 63] Because we can control particle size and spacing independently and over a wide range, we chose to demonstrate the application of this process to the growth of multi-walled carbon nanotubes.

Prior to the growth of catalyst nanoparticles, silicon nanowells were subjected to a 12 h thermal oxidation at 1000 ^{o}C under air and silanized with octadecyltrichlorosilane to avoid poisoning the catalyst by diffusing silicon or fluorine.[64] Iron or nickel chloride was loaded into nanowells and subjected to hydrogen reduction. Solution concentrations between 10 mM and 1.1 M were used to generate nanoparticles with diameters ranging between 4 and 20 nm.

The substrate was then heated to 750 ^{o}C under 5% hydrogen in Ar under a total flow of 1900 sccm. A carbon source was supplied for 10 min by adding 100 sccm of ethylene to the mix. After growth the tube was oven cooled to room temperature and substrates were characterized under SEM and TEM. Figure 2.10(a) clearly demonstrates the low percentage of active nanoparticle catalysts, ~0.5%. This low catalyst activity is similar to the catalyst activity in most carbon nanotube CVD synthetic techniques.[65] The most successful method developed was to utilize the water assisted carbon nanotube 'supergrowth' method.[60]

The supergrowth technique adds a low concentration of water vapor to the carbon nanotube growth mix. At high temperatures water vapor acts as a mild oxidizing agent and in carbon nanotube supergrowth water enables carbon nanotubes to grow to mm lengths. The occurs as waters serves to selectively oxidize the amorphous carbon which builds up around catalyst

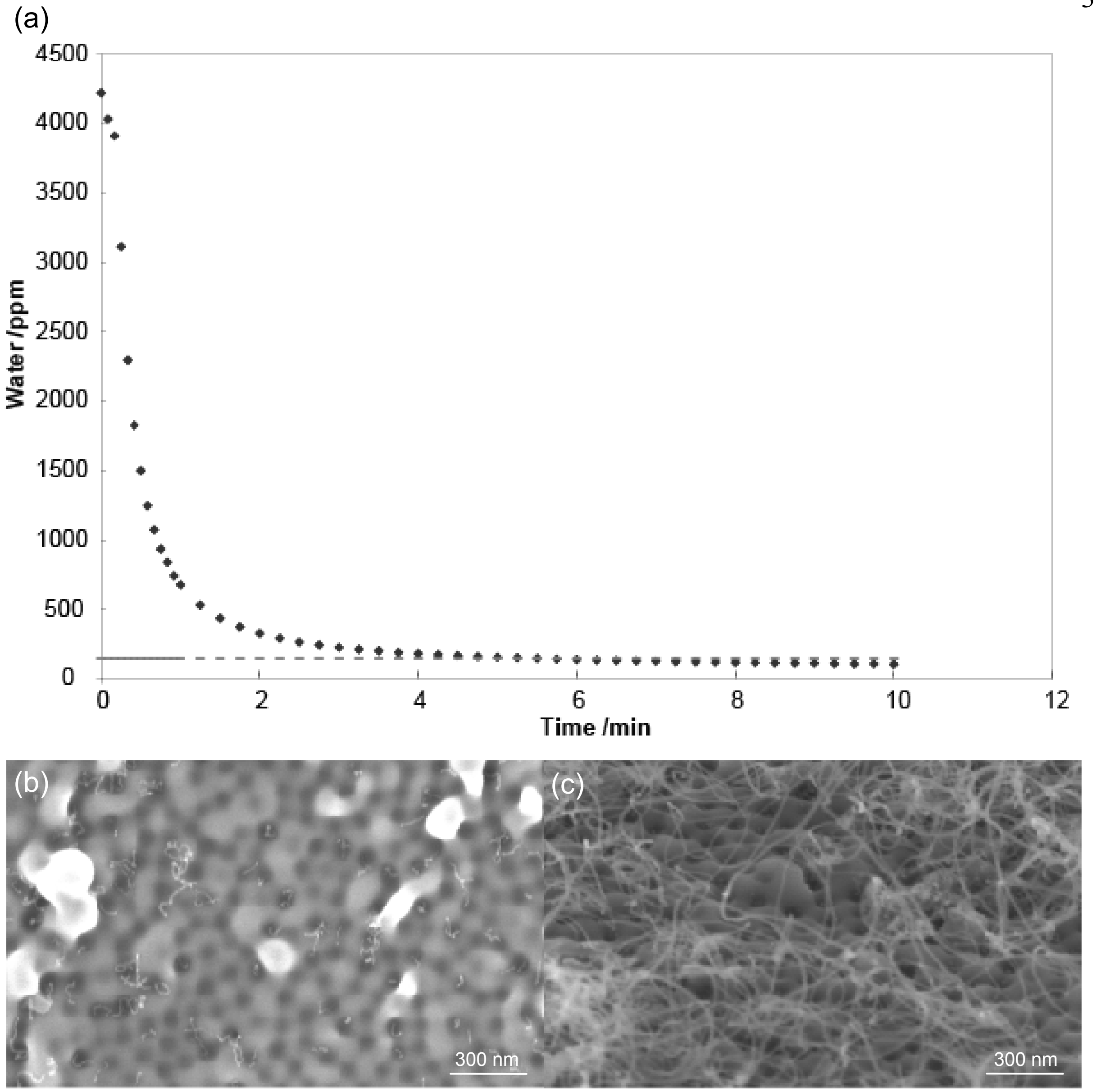

Figure 2.10: (a) Water concentration vs. time during carbon nanotube supergrowth. The line represents the previously reported water concentration during supergrowth. SEM of carbon nanotubes (b) without water and (c) with water.

particles and halts or prevents carbon nanotube growth, while being too mild and in too low a concentration to oxidize the more stable carbon nanotube structure. This technique has been demonstrated to yield extremely high carbon nanotube growth efficiency and lengths.[60]

In our version of this method, the addition of ethylene to the growth mixture was immediately preceded by a 1 min pulse of Ar through a water filled bubbler, which raised the partial pressure of water vapor in the tube furnace to ~50,000 ppm (measured by a relative humidity sensor (SHAW Grey Spot Hygrometer)). Ethylene flow then proceeded while the relative humidity was monitored. The ethylene was shut off when the measured water concentration fell below 50 ppm (after ~10 min).

By using a water pulse we increased the H_2O partial pressure at the beginning of the growth in order to prevent the formation of either amorphous carbon or carbon nanotubes around the catalyst particles. As the growth procedure continued the H_2O partial pressure fell through a zone where carbon nanotube supergrowth occurred. SEM characterization revealed a much higher catalytic efficiency of tube growth, with ~80% catalyst particles active. This result compares well to reported the reported catalyst efficiency under supergrowth conditions.[65]

2.4 Conclusion and Future Work

In summary, we have developed a technique for the fabrication of nanowells with zL volumes and have demonstrated how these wells provide a general method to confine chemical reactions and to synthesize nanocrystals. Laser-assisted embossing provides a relatively fast and easy method for the patterning of high densities of nanowells in silicon. Limitations of this route to nanocrystals include the relatively low concentrations of synthesized nanoparticles and the relatively small areas of silicon which can be easily embossed.

Because our method can produce isolated nanoparticles, detailed studies of the properties of individual particles are now possible. We anticipate that these reactors can also be used to synthesize new types of nanoscale materials at high temperatures. This combination of top-down nanoscale patterning and bottom-up chemical synthesis shows significant promise for the growth and parallel assembly of individual nanocrystals with complex properties.

Chapter 3

Nanoparticle Growth in Tantalum Oxide Nanowells Fabricated by Anodization

3.1 Background

Chapter 2 demonstrates how Si nanowells are used to synthesize nanoparticles by confining a solution to zL volume droplet. Although the simple processing, materials, and controllable surface chemistry of silicon made it a nearly ideal substrate, the embossing technique generates only 10^9 nanowells on silicon substrates which limits the technique to small scales; even in that case the small quantity of nanoscale material makes characterization difficult and time consuming. Recently, anodized tantalum oxide membranes were reported as a potential structure for growing zL nanowells.[66]

Although no growth mechanism was reported, the empirical results are quite similar to results obtained in anodized aluminum oxide (AAO). Under very specific conditions, electrochemical anodization of aluminum films results in self-ordering of AAO structures into an aligned nanoscale hexagonal close packed array of pores.[9, 11-17] The spacing of pores depends linearly on the applied voltage, and self-ordering occurs at high electric fields, typically at voltages just below the breakdown potential of the oxide barrier layer in that electrolyte.[16] After the AAO membrane is dissolved away, the remaining aluminum film has a HCP dimpled structure. By varying the electrolyte solution composition, voltages between 15 and 195 V have been successfully used to grow ordered AAO membranes with cell spacings between 50 and 600 nm.[9, 16, 17] Depending on the conditions, growth times ranging from 2 h to 36 h have been used to grow porous membranes many hundreds of microns in length.[17] Theoretical analyses of the AAO growth continue to investigate the detailed mechanism of the self-ordering process.[9, 15-17, 67]

In the tantalum system, anodization voltages between 12 and 20 V were reported to generate a detachable dimpled structure of amorphous Ta_2O_5 on the tantalum substrate. The spacing of the dimples was reported to be linearly dependent on the applied voltage, with wells ranging from 30-55 nm in diameter, and about 13 nm deep.[66] Compared to embossed silicon nanowells, tantalum oxide films have three potential advantages: square inches of uniform substrate, variable nanowell diameter and depth, and the transfer of transparent nanowell films to other substrates for additional processing and analysis.[66, 68, 69]

We have investigated the detailed growth mechanism of Ta_2O_5 nanoscale dimples, used them as nanowells to grow nanoparticles by confined precipitation, and examined the influence of one nanoparticle on the precipitation of another. We have further applied these tunable large area nanowell substrates to investigate details of nanowell loading by discontinuous dewetting.

3.2 Tantalum Oxide Nanowell Growth

Previously reported Ta_2O_5 nanowells were grown in an aged commercial tantalum electroetch solution, between 12-20 V.[66, 68, 69] Tantalum films were used as the anode in a classic two electrode electrochemical cell. The tantalum film reacted at 6 V in a 9:1 solution of H_2SO_4:HF for several hours to electropolish the tantalum surface and to 'age' the solution, increasing the concentration of TaF_7 while decreasing the concentration of HF. Then the voltage was raised to 12-20 V for 20 min to grow the nanowell tantalum oxide film. This technique varies from the commercial tantalum electropolishing recipe only in the age of the solution and the applied voltage; commercial tantalum electropolishing solution uses fresh electrolyte and 3-6 V.

In our work, amorphous tantalum oxide dimples were grown by electrochemical anodization of a tantalum film (Aldrich) in a standard two-electrode cell (Fig. 3.1). A 300-µm thick tantalum film was connected to the positive terminal of a DC power supply (Agilent E3612A), while a Pd wire (Aldrich) was used as the counter electrode. Tantalum films were electropolished to a

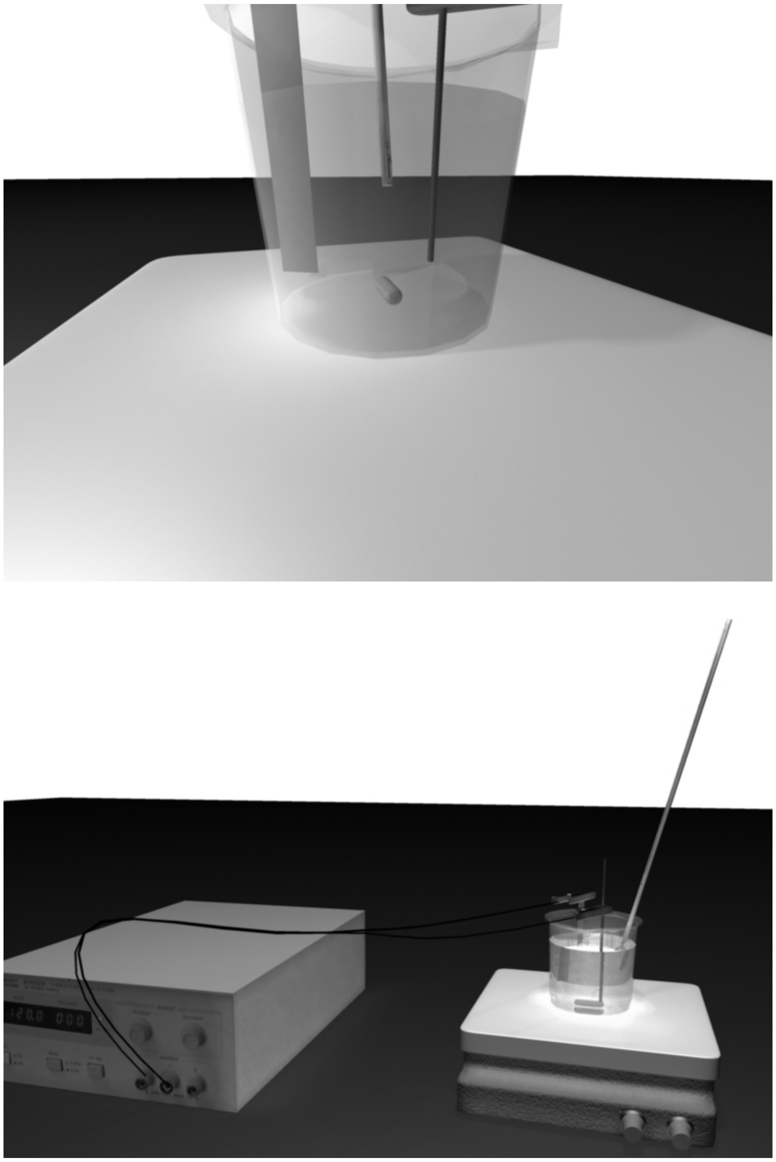

Figure 3.1: Cartoon of the two electrode electropolishing setup used for anodization. A tantalum anode is held in an electrolyte bath, while a Pd wire serves as the cathode. The electrodes are hooked to a DC power supply capable of supplying 500 mA up to 90 V.

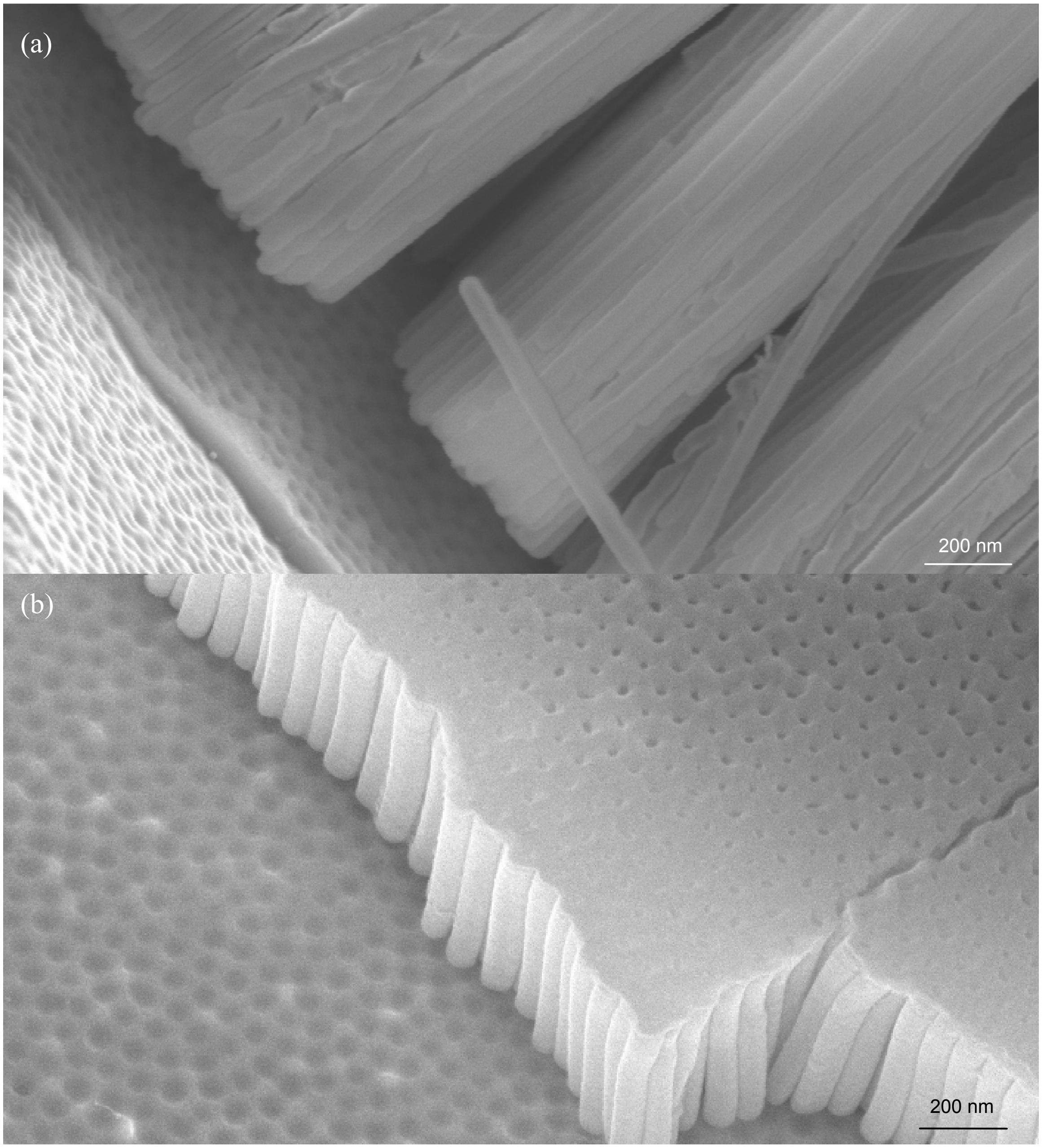

Figure 3.2: SEM image of 30-V Ta_2O_5 nanowells and nanotubes in (a) cross section and (b) from above.

mirror finish in a 9:1 H_2SO_4:48% HF at 6V for 20 min in order to reduce the surface roughness of the tantalum film. The films were then rinsed in 18 MΩ water and dried under a stream of nitrogen, before being immersed in a 50:1 concentrated H_2SO_4:49% HF mixture and anodized at 30 V for 20 min with a current density ~150 A/m^2. Anodization progress was monitored by recording the current-time transient. This process formed ordered tantalum oxide nanotubes (elongated nanowells) emerging from nanoscale dimples in a thin oxide film (Fig. 3.2 and Fig. 3.4). Because these arrays of tubes were only weakly bound to the surface, they could be easily removed by rinsing and sonication in water, or by stirring the solution during the electroetching, to leave a dimpled Ta_2O_5 barrier oxide over the tantalum film. For the purposes of nanowell fabrication, the substrates were anodized in a stirred solution in order to increase nanowell uniformity. The investigation of the Ta_2O_5 nanotubes is presented in Chapter 4. We observed that aging the electroetching solution was not required if the HF concentration was reduced; volume ratios between 100:1 and 20:1 H_2SO_4:HF could be used to make nanowells. Nanowell spacing and diameter were found to be linearly dependent on voltage between 10-90 V, although self-ordering was only observed between 15-35 V.

When tantalum anodization was resumed, the dimples nucleated the growth of new nanotubes.[9] By optimizing the anodization time, temperature, voltage, solution concentration of HF, H_2O, and H_2SO_4, nanowell uniformity and depth were tuned. Under optimized conditions, the dimpled tantalum substrate was anodized at 30 V a second time in an unstirred 60 ^oC dilute 1:5:125 HF:H_2O:H_2SO_4 mixture. These conditions lead to smooth nanotubes which grew at ~80 nm/s; nanowell depths were tuned by altering the anodization time between 0.5 s and 1.5 s. The range of optimized parameters was narrow. For example, anodization for 1 s at 63 ^oC grew a

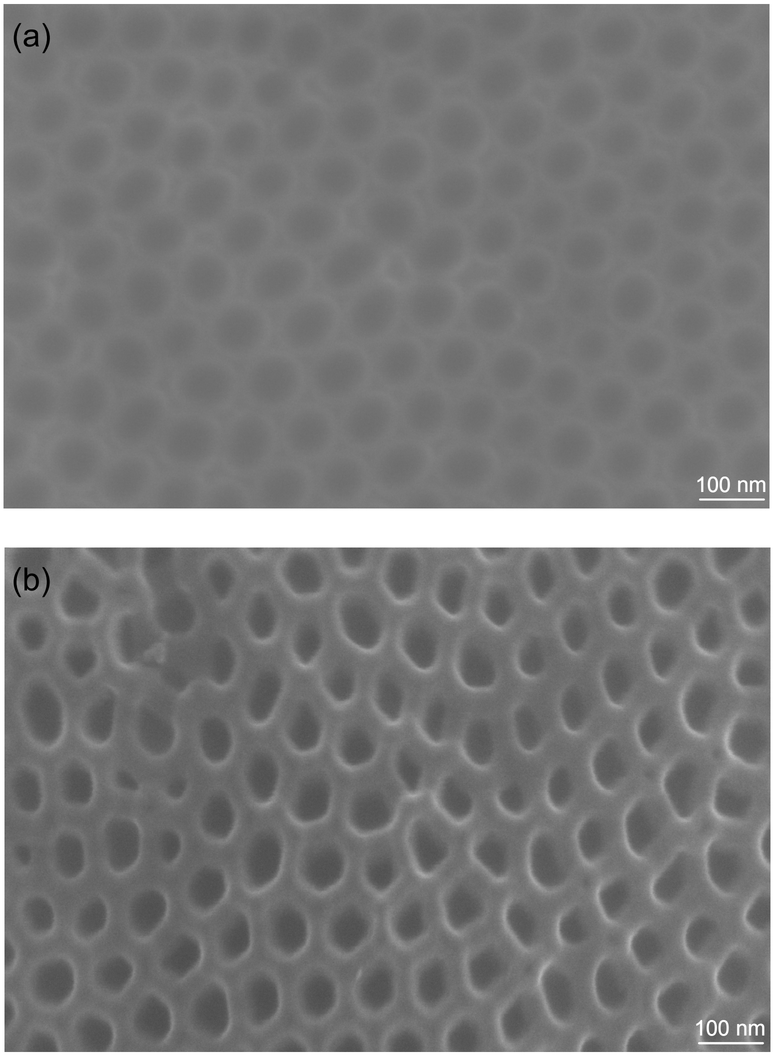

Figure 3.3: SEM images of 30-V nanowells (a) prior to, and (b) after secondary anodization. Nanowell depth increased from ~13 nm to ~45 nm.

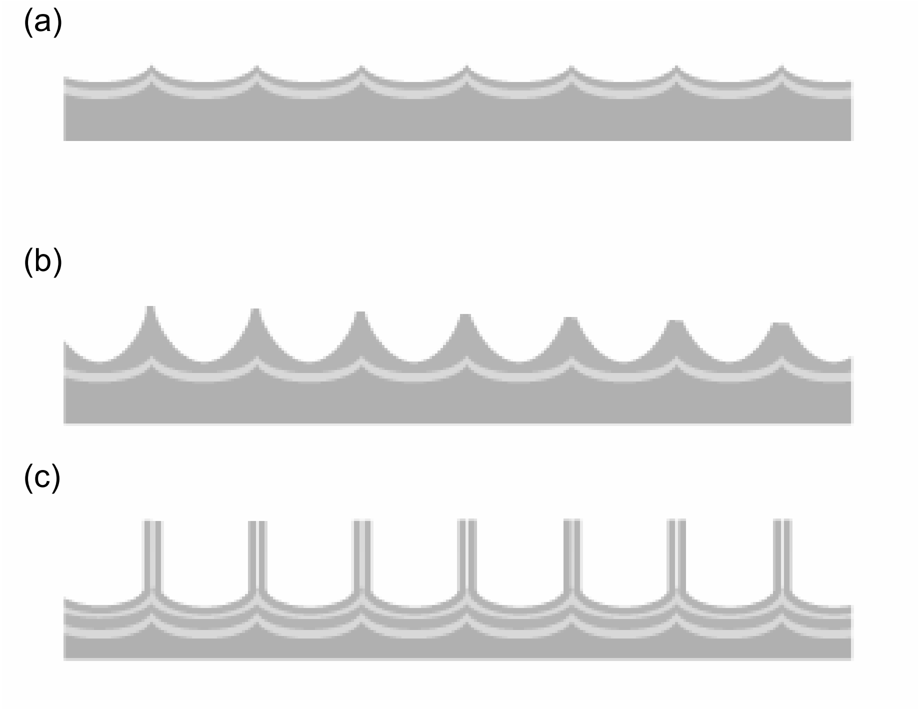

Figure 3.4: Schematic of tantalum oxide nanowell structure. (a) Dimpled tantalum oxide after first anodization. The light gray layer is water soluble tantalum fluoride. (b) Tantalum oxide nanowells grown by a short second anodization of (a) at 60^{o}C. (c) Tantalum oxide nanotubes grown after a longer second anodization. A tantalum fluoride between the nanotubes and the barrier oxide causes the nanotubes to leave the surface when agitated.

rougher more crystalline appearing material, while anodization at 58 °C grew an oxide film across the substrate rather than growing nanotubes.

3.3 Nanoparticle Growth

3.3.1 Nanowell Surface Chemistry

For nanowell substrates to function as templates for growing materials-general nanoparticles, the surface chemistry must be inert to precursor materials. As prepared, tantalum oxide nanowells were extremely hydrophilic (contact angle ~0^o) and reactive to the metal salts typically used to grow nanoparticles in silicon nanowells. To control the surface chemistry of the tantalum oxide nanowells, we used a modified chemical priming treatment, followed by a vapor phase silanization.[70] The substrate was immersed in a room temperature solution of 4:1:1 H_2O:NH_2OH:30% H_2O_2 for 5 s. and rapidly rinsed with 18 MΩ water. This priming step striped the top surface oxide layer, leaving exposed hydroxyl groups. Standard oxygen plasma treatment was insufficient for this task on tantalum oxide while the full 15 minute immersion in 70 °C solution called for in the original prep caused complete dissolution of the oxide film. The substrate was then placed in a desiccator with ~10-20 μL of octadecyltricholosilane and allowed to react under house vacuum for 12-24 hours. This procedure generated a hydrophobic organic adlayer that prevented adsorption of metal salt precursors to the template surface. Without this adlayer, nanoparticles nucleated over the entire substrate and were polydisperse in size. After only a day exposed to the air, substrates were no longer effectively passivated and nanoparticles began nucleating randomly on dewetting. Storage under house vacuum was sufficient to avoid this degradation.

3.3.2 Nanowell Geometry

Dimpled substrates formed by the first tantalum anodization could not be used to grow nanoparticles by discontinuous dewetting. From our previous work, the large size of the nanoparticles suggested that the solution within a hydrophobic nanowell was confined to a sphere defined by the curvature of the underlying nanowell. Thus, when the radius of curvature of the nanowell exceeded the separation between nanowells, adjacent droplets overlapped and dewetting could not be used to load solution into the nanowells (Fig. 3.5). 30-V tantalum oxide dimples had a diameter of ~85 nm and a depth of ~15 nm, which represents a sphere with a diameter of ~150 nm. The secondary anodization procedure was developed to address this issue. The 0.5-s anodization generated nanowells ~85 nm wide and ~40 nm deep, with a radius of curvature of ~40 nm. This curvature was enough to avoid overlap with neighboring nanowells, and allowed nanowell loading by discontinuous dewetting. Loading into higher aspect nanowells did not work, most likely because of the high pressure required to force an aqueous solution into a narrow hydrophobic pore.

3.3.3 Nanoparticle Loading and Reaction

Silane passivated nanowells were loaded with molecular precursors as in Chapter 2.[35, 58] In a typical reaction, substrates were immersed perpendicular to the surface of a precursor solution of interest and withdrawn at 50 μm/s. Metallic and metal oxide nanoparticles were grown in nanowells by dissolving metal chlorides in water and loading the solution into hydrophobic nanowells. In the absence of nucleation points within the nanowells, only one crystal formed on precipitation.[35, 58]

Substrates were then placed in a 1” tube furnace, where they were heated to 90% of the melting temperature of the bulk precursor under a hydrogen atmosphere (10 ^{o}C/min ramp rate,

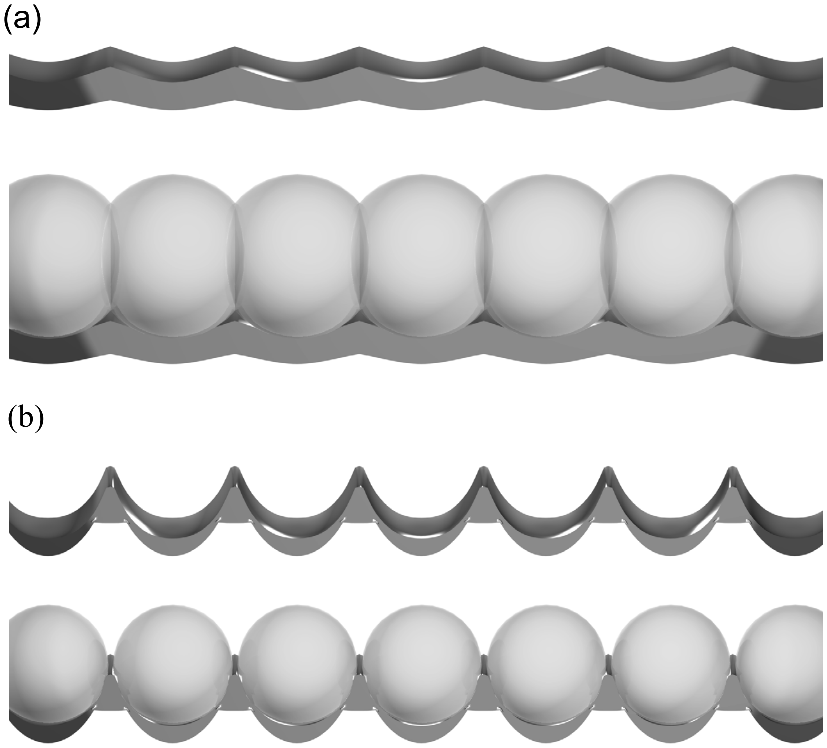

Figure 3.5: Diagrams detailing how radius of curvature effects nanowell loading. In case (a) the shallow nanowells are packed too closely together. When the wells are loaded by discontinuous dewetting, they overlap, and discontinuous dewetting fails. In case (b) the nanowells are deep enough to isolate the solution spheres without being so deep that filling is unfavorable.

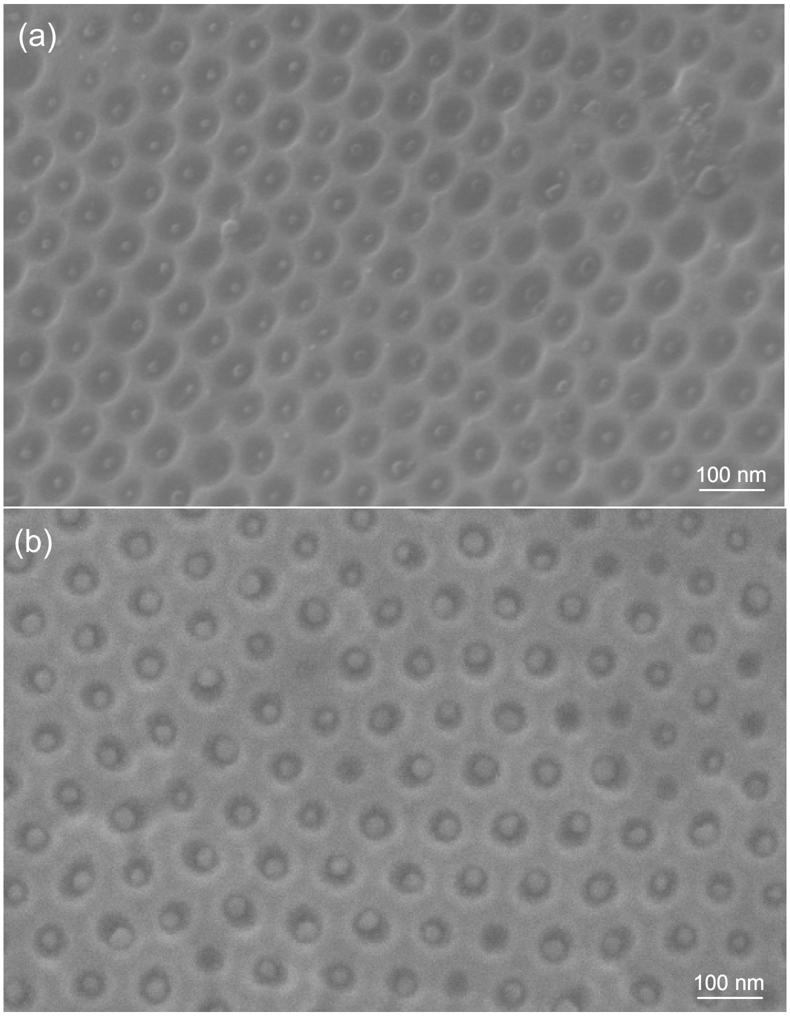

Figure 3.6: SEM images of passivated Ta_2O_5 nanowells filled with (a) 1 M and (b) 5 M NaCl solutions.

held for 1 h). The principle limitation on this system was the relative fragility of the tantalum oxide nanowell substrate. Tantalum oxide nanowells were not as robust as silicon nanowells; temperatures over ~600 ^{o}C caused crystallization of the oxide, and heating over 500 ^{o}C in oxygen oxidized the underlying tantalum substrate and left an oxide powder in the reactor.

3.3.4 Nanoparticle Growth in Nanowells

All substrates were tested for nanowell loading by dewetting a 1-5 M sodium chloride solution. Figure 3.6 shows that the size of nanocrystals precipitated in tantalum oxide nanowells depends on concentration, just as nanocrystal growth in Si nanowells do.

3.3.4.1 Gold Nanoparticles

Gold nanoparticles were grown by filling the wells with a 0.01-1.0 M solution of $HAuCl_4$ by discontinuous dewetting at a rate of 100 μm/s. The samples were then heated to 225 ^{o}C in a tube furnace under a 50% H_2/Ar atmosphere. Substrates were heated at 10 ^{o}C/min, held at the reaction temperature for 60 min, and then oven-cooled to room temperature. A final wash in H_2O removed any residual precursors.

SEM confirmed the presence of single gold nanoparticles in individual wells (Fig. 3.7). TEM imaging was used to characterize the nanoparticle size and dispersion at the different concentrations. HR-TEM was used to confirm elemental composition and crystal structure. Sample preparation was accomplished by sonicating nanoparticle loaded tantalum oxide nanowell substrates in a small volume of ethanol and examining flakes of oxide nanowells in the TEM. Nanoparticles were generally observed in each nanowell. Because tantalum has a very high Z-number, we were unable to observe elements lighter than atomic number 73 through the amorphous film.

3.3.4.2 Magnetic Nanoparticles

This nanoparticle synthesis procedure worked well for a wide range of metal or metal oxide nanoparticles. We demonstrate with iron, cobalt, and nickel. In the absence of stabilizing ligands, nanoparticles were found by XPS to oxidize in atmosphere prior to characterization. Iron oxide nanoparticles were grown by loading 0.01-1 M iron(II) chloride solutions and reducing at 600 ^{o}C, yielding particles with diameters ranging from 5 nm to 25 nm. Cobalt precursor nanoparticles were grown from 0.1 M solutions of cobalt(II) acetate and held at 100 ^{o}C under argon for 30 min to dehydrate the nanoparticles. Particles were then heated to 250 ^{o}C under hydrogen for final conversion to cobalt metal, which oxidized when exposed to air. Nickel oxide nanoparticles were made from 0.1 M solutions of nickel(II) chloride held at 100 ^{o}C under argon to dehydrate, followed by heating at 600 ^{o}C under hydrogen to reduce to nickel metal which oxidized when exposed to air.

3.3.4.3 Core-shell and Intermetallic Nanoparticles

To increase the versatility of the nanowell synthetic platform, we experimented with loading multiple precursor materials into the nanowells and we found that we could load additional material into nanowells. The hydrophobic adlayer remained stable enough to prevent non-specific adsorption after hydrogen reduction up to 300 ^{o}C. When we grew a second set of nanoparticles, the first set acted as the sole nucleation point within the nanowells. The new precursor precipitated around the previous nanoparticles on solvent evaporation. HR-TEM and EDX characterization indicated that after reduction the new nanoparticles formed an alloy, likely due to the high temperature of the reduction step. Thus by loading and reducing one material, then loading and reducing a second material, we were able to make intermetallic nanoparticles (Fig. 3.8).

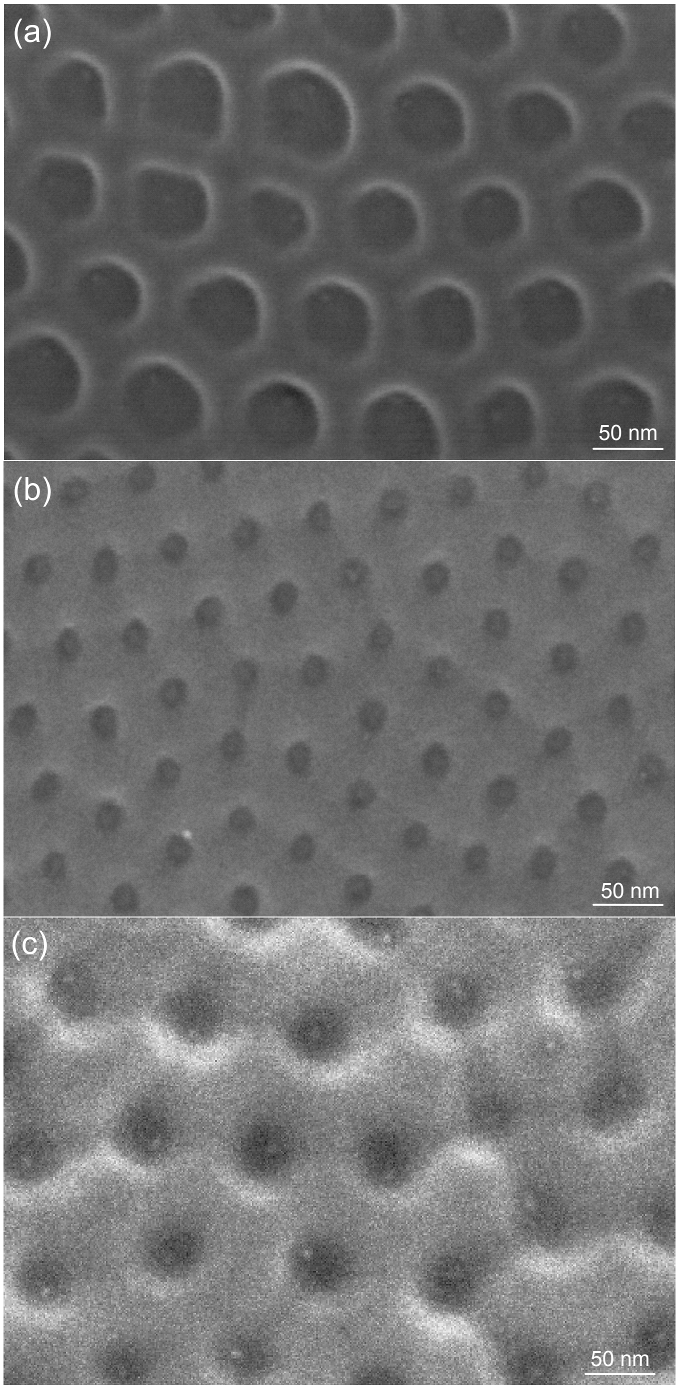

Figure 3.7: SEM images of metal oxide nanoparticles. (a) iron oxide nanoparticles grown from 100 mM iron chloride solutions in 30-V nanowells. (b) 1 M iron oxide nanoparticles in 20-V nanwells. (c) 100 mM cobalt oxide nanoparticles in shallower 30-V nanowells.

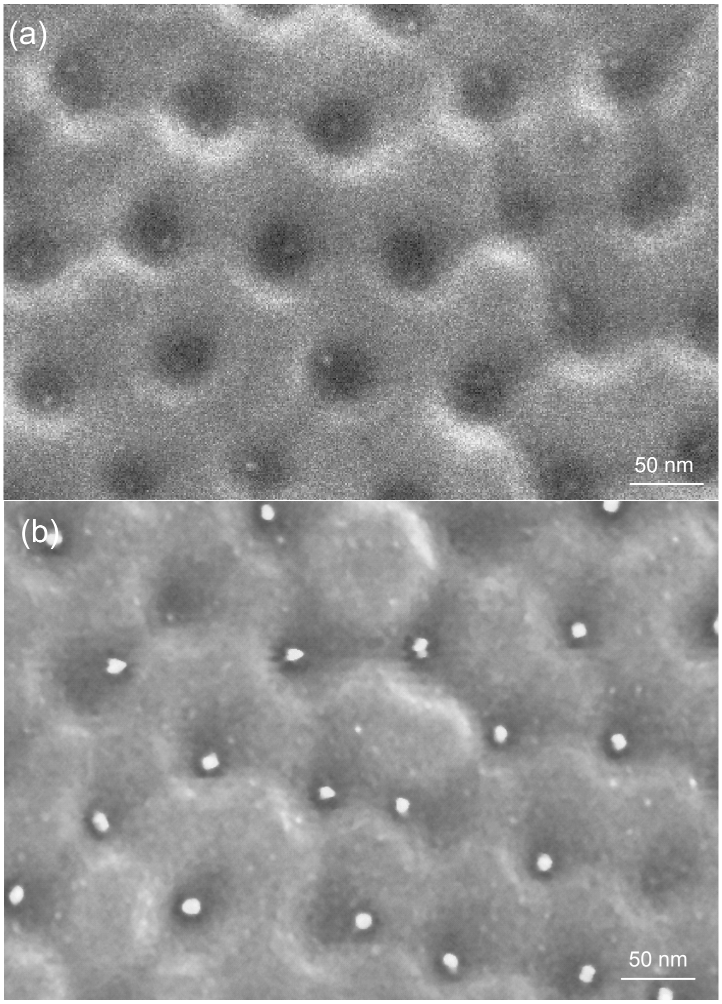

Figure 3.8: SEM images of (a) cobalt nanoparticles and (b) cobalt nanoparticles which have been dewetted with Au precursor and reduced by hydrogen.

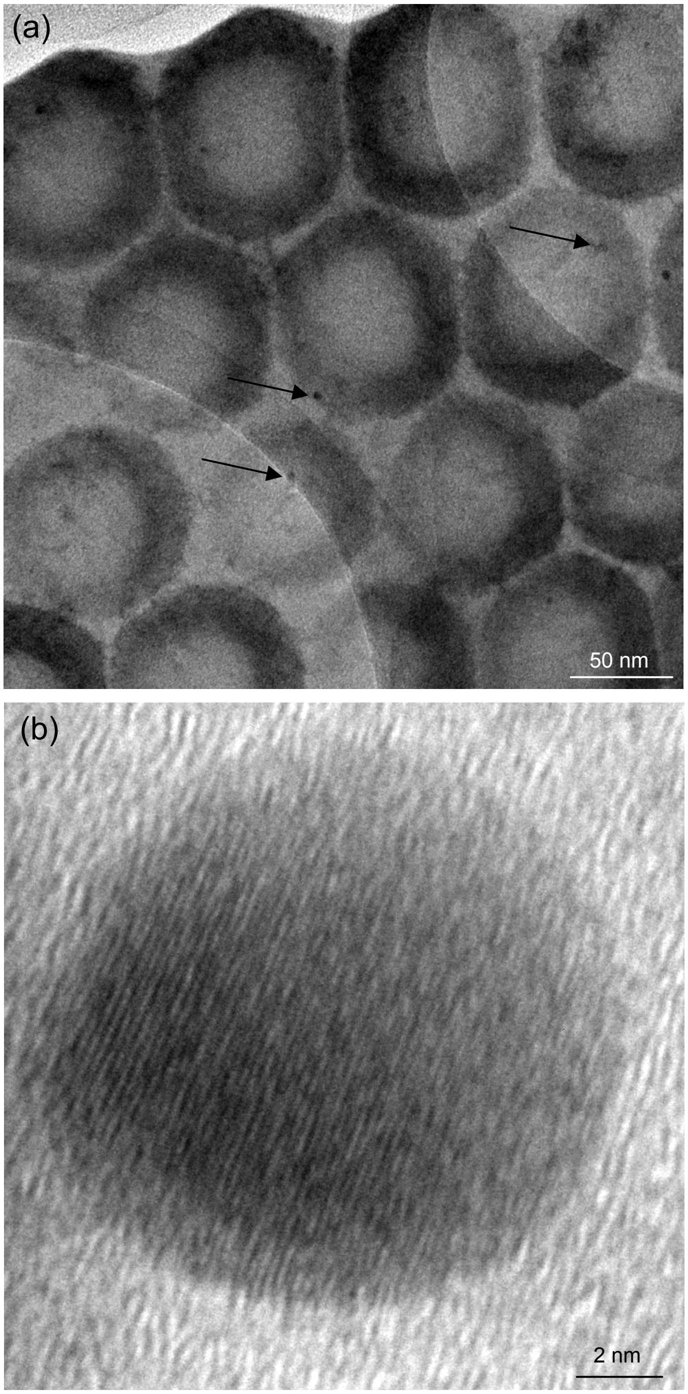

Figure 3.9: TEM images of (a) 3 nm Au nanoparticles in nanowells, and (b) an 11 nm gold nanoparticle reacted with thallium metal. The major lattice fringes are spaced by 2.4 Å, and the minor fringes by 2.25 Å, a close match to $AuTl_2$ at 2.29 Å.

In a typical reaction, 0.1 M hydrogen tetrachloroaurate was used to grow the initial 10-nm diameter nanoparticles. The Au precursor nanoparticles were reduced in 100% hydrogen at 225 ^{o}C to create Au nanoparticles. A 0.1 M TlCl solution was then loaded into the nanowells and allowed to precipitate. After hydrogen reduction at 400 ^{o}C, the substrate was sonicated into ethanol and dispersed on a TEM grid for analysis. Only a single nanoparticle was visible within each nanowell (Fig. 3.9). EDX analysis indicates the presence of Au and Tl, but the 2.29 Å and 2.4 Å lattice fringes observed in HR-TEM did not match Au, Tl, or the thallium oxides. The closest match was to $AuTl_2$ (PDB 01-071-7581). Au and Tl form intermetallic compounds, and thallium likely dissolved into the small Au nanoparticle during the reduction reaction. In some nanoparticles a shell of amorphous material was observed around the $AuTl_2$ core, and some Tl might have reacted with atmospheric oxygen and precipitated out of the intermetallic nanoparticle.

3.4 Summary

We have discovered the general mechanism of tantalum oxide nanodimple formation and leveraged this chemistry to generated square inches of tantalum oxide nanowells. The tunability of these nanowells allowed us to investigate the parameters of nanoscale discontinuous dewetting and we found that the radius of curvature is the critical component for nanowell precipitation. We used the tantalum oxide nanowell film to examine nanoparticles within nanowells by TEM. This revealed that precipitation in the presence of an existing nanoparticle occurs preferentially around that nanoparticle. We conclude that the existing nanoparticle acts as the nucleation point for further nanoparticle growth, and that the high temperature hydrogen reduction and low melting points of small nanoparticles favors the formation of intermetallic nanoparticles.

Chapter 4

Anodic Synthesis of Ta_2O_5 Nanotubes and Conversion to TaS_2 Inorganic Fullerene Nanotubes

4.1 Introduction

One class of templates commonly used for nanotechnology applications are porous anodized alumina membranes. In contrast to the typical sponge-like structure of most other porous anodized metal oxides, anodized alumina forms discrete highly aligned pores when anodized in certain dilute acids; the size of those pores depends linearly on the applied voltage.[71] When anodized at voltages approaching the breakdown potential of the oxide in that electrolyte, the pores self-order into an HCP array. When anodized well above the breakdown potential of the oxide, the aluminum "burns" as aluminum oxide breaks down locally. Current density in that area increases dramatically, and thick layers of HCP porous aluminum oxide occasionally grows in those areas of high current density.[16]

4.1.1 Growth of Porous Aluminum Oxide

Although the detailed mechanism of AAO ordering has been a subject of debate and experimentation for the last five decades, empirical investigations have revealed the basic electrochemistry of growth.[9, 12-17, 67] On a flat substrate, pore growth nucleates at defects in the passivating oxide layer, which is thin and non-uniform and supports an electric field gradient of several megavolts per cm. During pore growth, the electric field and ionic current density at the pore bottom should be larger than that between the pores due to a decreased oxide thickness. Al^{3+} ions are formed at the oxide-metal interface while O^{2-} ions are formed in a rate-limiting water-splitting reaction at the oxide-electrolyte interface.

$$\mathrm{Al(s)} \rightarrow \mathrm{Al}^{3+}(\mathit{oxide}) + 3\mathrm{e}^{-} \qquad (1)$$

$${}^{3}/_{2}\mathrm{H_2O}(l) \rightarrow 3\mathrm{H}^{+}(aq) + {}^{3}/_{2}\,\mathrm{O}^{2-}(\mathit{oxide}) \qquad (2)$$

Both ions migrate into the barrier oxide layer and react to form a new oxide within the layer, while the protons generated by the water splitting reaction at the oxide-electrolyte interface locally dissolves the oxide at the bottom of the pore:

$$^{1}/_{2}Al_2O_3(s) + 3H^+(aq) \rightarrow Al^{3+}(aq) + ^{3}/_{2}H_2O(l) \qquad (3)$$

Stoichiometric analysis has indicated ~70% of the current density is used to generate Al_2O_3, while the remaining 30% represents reaction (3).[72, 73] To complete the circuit, hydronium ions can also migrate to the cathode and leave the cell as $H_2(g)$. Stable oxide pores are formed because reaction (2) occurs preferentially in the high electric field at the bottom of the pores generating the protons used in reaction (3). Under certain voltage and electrolyte conditions, reactions (1), (2), and (3) are in a steady state, the thickness of the barrier oxide remains constant, and the pores grow continuously. The majority of the oxide is deposited in the walls of the pores by horizontal diffusion of the mobile Al^{3+} ions through the barrier oxide.[9] It has been suggested that the ordering into HCP arrays depends on equilibration between the expanding oxides of competing pores.[74] Under this model the increased pore order observed near the breakdown potential of the oxide is considered an effect of moderate oxide expansion, while at higher voltages reduced order is observed because of excessive volume expansion and dielectric breakdown. By choosing an appropriate acid the breakdown potential of the oxide can be moved to certain points between 28 V and 196 V. AAO pore spacing depends linearly on the anodization voltage, with a correlation parameter of ~2.5 nm/V. Each oxide breakdown voltage allows the formation of a certain diameter of HCP porous alumina.

Under high-field anodization, HCP AAO pores occur over a wide range of voltages in a single electrolyte. High-field anodization occurs between 120-150 V in oxalic acid electrolyte which has been used to anodize alumina for approximately 20 amp/h and has a reduced conductivity. These conditions were far harsher than the self-ordering "mild anodization" condition at 40 V, and rapidly growing self-ordered HCP pores were found to grow at a spacing linearly dependent on the growth voltage.[9] The correlation parameter of this voltage dependency is 2.0 nm/V, which does not match the 2.5 nm/V dependence of mild anodization.

4.1.2 Other Ordered Anodized Metal Oxides

AAO membrane structures have been used as templates for the electrodeposition of a wide variety of nanowires, nanotubes, and nanostructures,[11, 34, 39] and the widespread applications of porous alumina have stimulated a search for similar behavior in other porous metal oxide systems.[75-80] A number of other valve metal systems have been observed to develop sponge-like porous structures under anodization. ZrO_2 has been observed to grow nanotubes[75, 81] and HfO_2 has demonstrated disordered pores with a voltage dependent cell spacing,[78] but only anodized TiO_2 nanotubes have been observed to self-order in a voltage-dependent fashion similar to AAO membranes. [10, 61, 75, 82-84] TiO_2 nanostructures have attracted a great deal of interest because of the photochemical applications that can be enhanced by structuring as nanotubes.[85],[61] Anodizing titanium films in dilute fluoride containing electrolytes has produced amorphous TiO_2 nanotubes with diameters that depend on the solvent viscosity and applied anodization voltage.[10, 61, 82, 84, 86] The growth mechanism is similar to that of AAO growth with the additional factor of direct chemical dissolution of the TiO_2 by F^- ions. Additionally, the lower ion mobility of Ti^{4+} through the oxide film prevents the horizontal diffusion of Ti^{4+} necessary to fill in the oxide between the tubes; thus anodization of titanium films yields nanotubes instead of a porous membrane. In the first reported work, dilute HF solutions were used as the electrolyte, and although the constant current revealed continuous growth of TiO_2, the resulting nanotubes were only ~500 nm long and their length was independent of anodization time. Because TiO_2 is soluble in HF, the balance of electrochemical growth with chemical dissolution of the nanotubes in solution resulted in nanotube lengths that saturated when the growth rate equaled the dissolution rate. By replacing the HF with an alternate fluoride source such as NH_3F or KF in an acidic solution, 4.4-μm TiO_2 nanotubes could be grown.[87] The reaction of F^- with water generates HF and OH^- and allows the relative concentrations of HF and F^- to be controlled by pH. Using an organic electrolyte such as ethylene glycol as solvent enabled controlled amounts of water to be added to the solution as a reactant, ensuring more precise control over F^- concentration; this modification further reduced the chemical dissolution rate of the nanotubes. Tubes up to 200 μm in length have been grown this way.[82]

Recent reports of the rapid electrochemical formation of HCP ordered voltage dependent 30-50-nm dimples in tantalum films suggested that voltage-tunable self-ordered porous tantalum oxide nanostructures could be grown.[66, 68, 69] Ta_2O_5 is a high- κ dielectric insulating material that has been under intense study for application in future CMOS technology.[68, 88-90] Nitrogen doped Ta_2O_5 has demonstrated potential as a visible light oxidative catalyst, [91] while Ta_2O_5 can act as a solid electrolyte for Li^+, which shows promise as an anode matrix material for Li ion batteries.[92, 93] These applications have all been shown to benefit from nanotube architecture in other material systems.[61, 83, 94, 95]

4.2 Tantalum Oxide Growth and Conversion

Amorphous tantalum oxide nanotubes were grown by electrochemical anodization of a tantalum film in a procedure similar to that outlined in Chapter 3. Anodization occurred in a H_2SO_4:HF solution, where the reaction time, applied voltage, temperature, and HF and H_2O concentrations were varied. In certain experiments, HF was replaced by another fluoride donating salt such as ammonium fluoride, tetrabutylammonium fluoride, or potassium fluoride. Because the anodized tantalum oxide layer is separated from the tantalum substrate by a thin layer of water-soluble TaF_3,[68] the nanotubes could be easily removed from the substrate by stirring, so the reaction was carried out in unstirred solution. Tubes were collected for characterization by sonicating in water for 10-s and dispersing onto substrates.

XPS and EDX characterization revealed that the stoichiometry of as-grown tantalum oxide nanotubes was approximately Ta_2O_5, with a small quantity of tantalum and a substantial fraction of fluorine. Annealing nanotubes under air at 400 °C was found to remove both these non-stoichiometric components. Glancing angle x-ray diffraction (GA-PXRD), HR-TEM, and selected area electron diffraction (SAED) indicated the as-grown Ta_2O_5 nanotubes were amorphous (Fig. 4.1(a)). After annealing at 750 °C for 12 h, the amorphous Ta_2O_5 tubes exhibited improved crystallinity with single 2-5-μm long grains but with no preferred crystal axis along the length of the tubes (Fig. 4.1(b) and (c))

4.3 Effect of Anodization Conditions on Ta_2O_5 Structure

4.3.1 Anodization Voltage

Nanotubes were grown between 10-90 V in a wide variety of solution concentrations. In all cases, a self-ordering regime was observed between 15-35 V. Similar to alumina and titania, Ta_2O_5 nanotube spacing and outer diameter were found to be directly proportional to the applied voltage, with a proportionality constant of 2.5 nm/V (Fig. 4.2). By removing the tubes and investigating the tantalum dimples in the substrate by SEM, the self-ordering regime between 15 and 35-V was determined, while at higher voltages (40-90-V) reduced ordering was observed. A

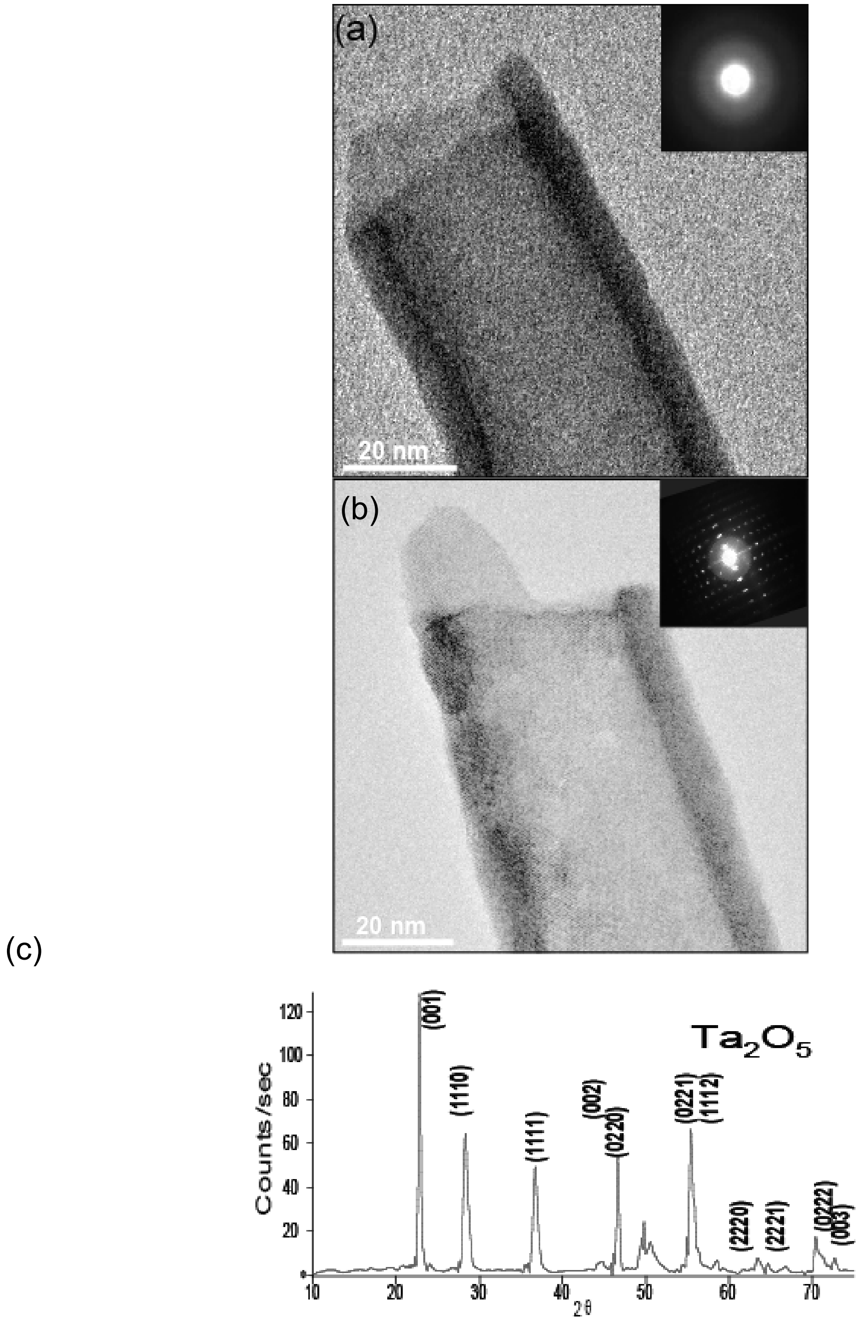

`

Figure 4.1: TEM images of (a) amorphous and (b) annealed Ta_2O_5 nanotubes and their corresponding SAED patterns (inset) and (c) the PXRD spectra of crystalline Ta_2O_5.

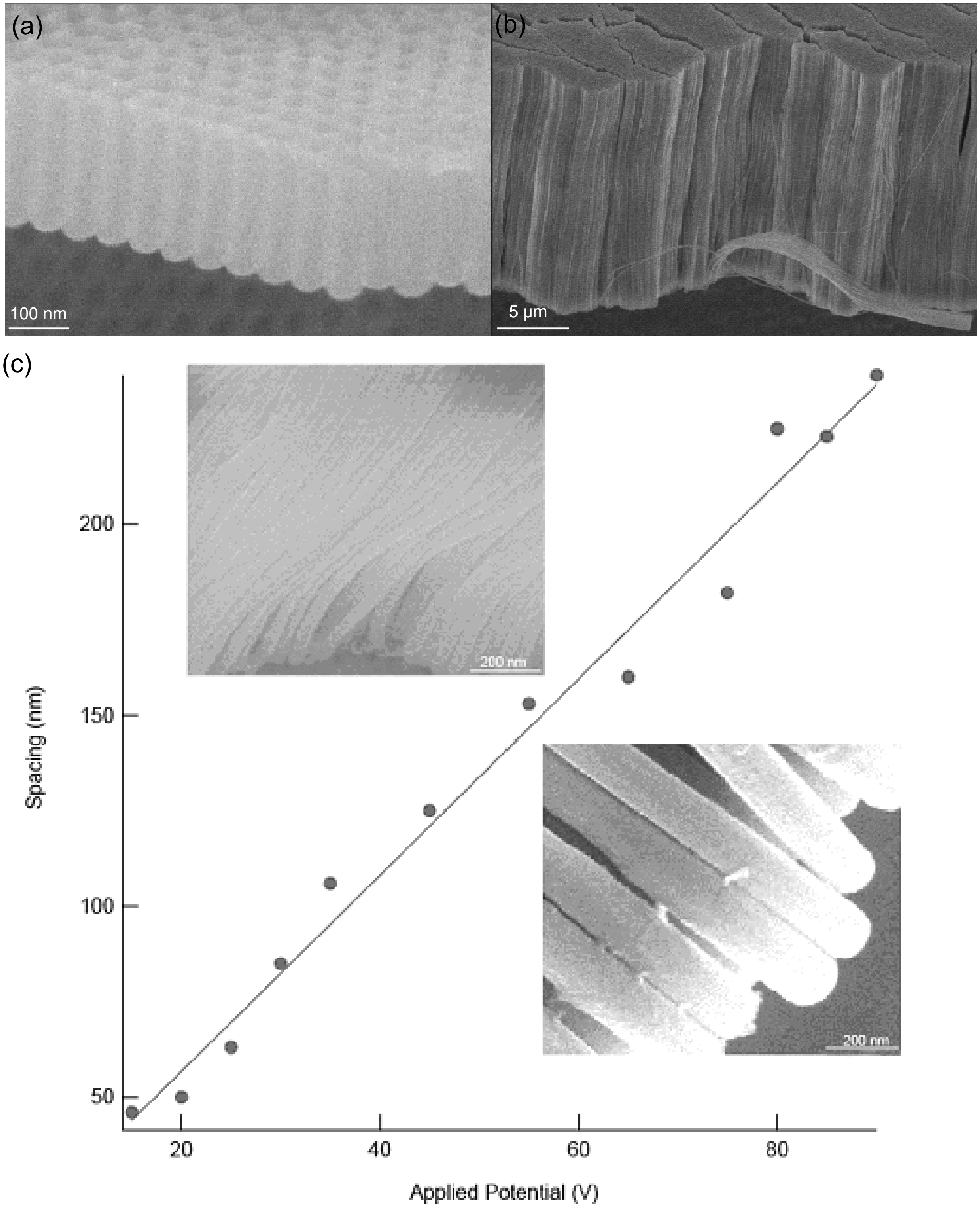

Figure 4.2: SEM images of (a) short and (b) long nanotubes grown at 30 V. (c) Graph of voltage vs. cell spacing with a 2.5 nm/V proportionality constant. Insets are SEM images at 15 V and 80 V growth.

2-h anodization at 50 V yielded submicron patches of HCP nanotubes, while a 4-h of anodization at 80 V showed polydisperse nanotubes with no ordering.

By varying the voltage during anodization, the nanotube diameter and ordering could be changed during the growth process. Figure 4.3 shows how the rate of change of voltage was the most important parameter. Reducing the voltage from 35 V to 25 V reduced the nominal nanotube outer diameter from 100 nm to 80 nm. A rapid change in voltage (5 V/s) produced to a rapid change in the nanotube diameter, which created a narrow band of high stress in the nanotube film. The reduced voltage caused the growth pores to divide, reorder, and split many tubes into two. When the voltage was rapidly increased, the existing tubes fractured away and separated from the growth zone as the growth pores rapidly increased in diameter. In contrast, a more gradual change in voltage (0.5 V/s) allowed more time for pores to reorder. On voltage reduction, many nanotubes split smoothly. On voltage increase, most nanotubes ceased to grow while others expanded their diameter, suggesting that growth pores competed rather than merged. Although not pursued in this work, such continuous control over nanotube diameter and optical density may have applications in photonic materials.

In contrast to porous alumina, Ta_2O_5 anodization in HF does not burn at higher voltages. At voltages above ~20 V there was a period of high current, but instead of burning, this high current occurred because a small portion of the electrolyte wicked up the tantalum substrate from the bath. During the initial stages of anodization, this liquid layer initially smoked and boiled off, and the high temperature increased the reaction rate and exceeded the amperage capacity of the power supply. The voltage typically stabilized within one minute as the extraneous solution boiled away and nanotube growth began.

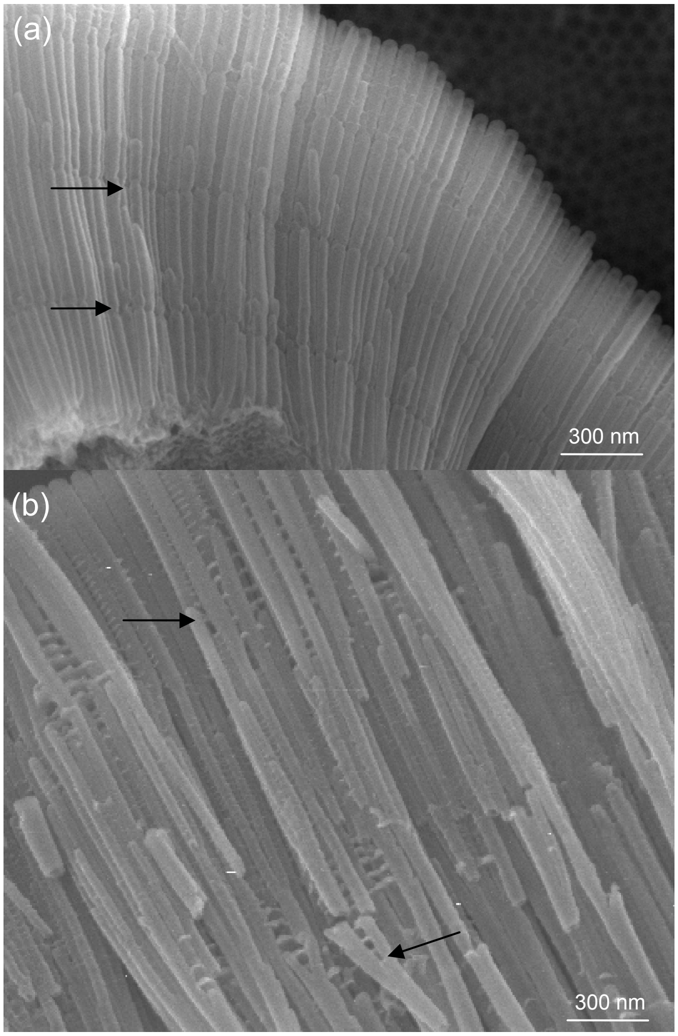

Figure 4.3: SEM images of nanotube reordering when voltage is changed (a) at 10 V/s, and (b) slowly at 0.5 V/s during growth. Arrows highlight regions of interest where (a) nanotube growth ceases when voltage is reduced at 10 V/s for a period of 10 seconds, and (b) where growth pores split and collapse when voltage is varied at 0.5 V/s.

Current density vs. time curves were recorded in order to examine the growth process. Figure 4.4 shows a typical curve at 30 V with features characteristic of the formation of ordered pores, where the current density peaks within the first 20 s and then falls of rapidly to a steady-state value.[16] Under most electrolyte conditions, that steady state current density was highest during growth at 30 V.

4.3.2 Electrolyte Parameters

4.3.2.1 Electrolyte Phase Diagram

A 30-V potential, chosen for its sustained self-ordering growth rate, was used to construct an HF:H_2O solution phase diagram for the reaction (Fig. 4.5). Electrolyte solutions ranging from 0-3.2 % w/w HF and 2-12 % w/w H_2O were prepared and held at 60 ^{o}C. 1-cm^2 areas of tantalum were anodized at 30 V for 10 min. Tubes did not grow at water concentrations less than ~3.5% at 1.6% HF. At lower HF concentrations, more water was needed to initiate growth. Conversely, at higher water concentrations, less HF was needed to initiate nanotube growth. Although nanotubes would not grow at any HF concentration under 0.14% to 6% H_2O, at 12% H_2O, 0.04 % HF was sufficient to grow nanotubes. In this case, the tubes were much less likely to separate. These results suggested that nanotube growth depended on the concentrations of fluorine ions in solution, which was non-linearly related to HF and H_2O concentration. Standard equilibrium models for fluorine ion concentration in this solution do not apply since concentrated sulfuric acid is a superacid, and pK_a values measured in aqueous solutions are not meaningful.[96]

4.3.2.2 Electrolyte Composition

The nanotube growth rate depended most critically on high water concentrations and low HF concentrations. At 12% H_2O and 0.22% HF, a growth rate of 8.5 μm/min was observed, which is

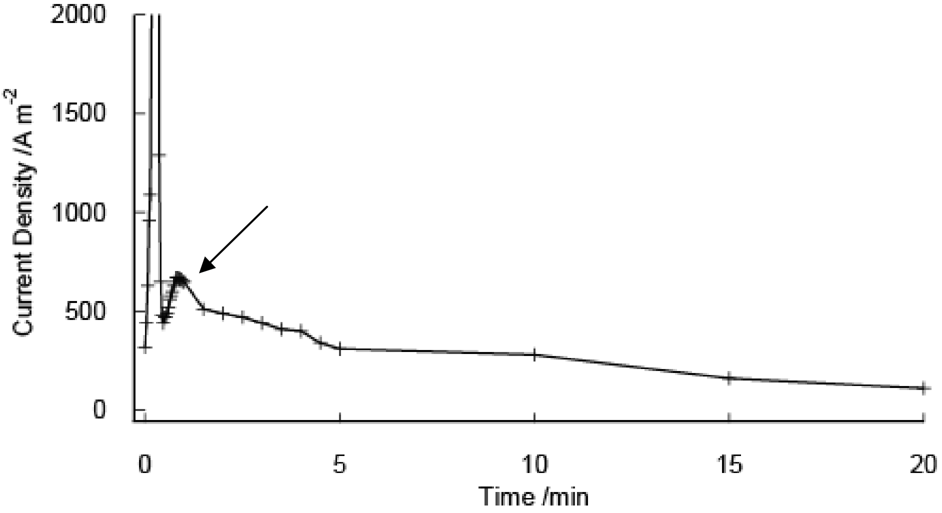

Figure 4.4: Typical current time transient curve for a 30-V anodization of a tantalum film at 0.25% HF, 4.3% H_2O. After initial saturation, the current density rises to a peak within a minute, before falling off to a steady state current. This initial growth peak (indicated by an arrow) is characteristic of pore ordering and is observed in both porous alumina and TiO_2 nanotube growth, although typically over longer time scales.

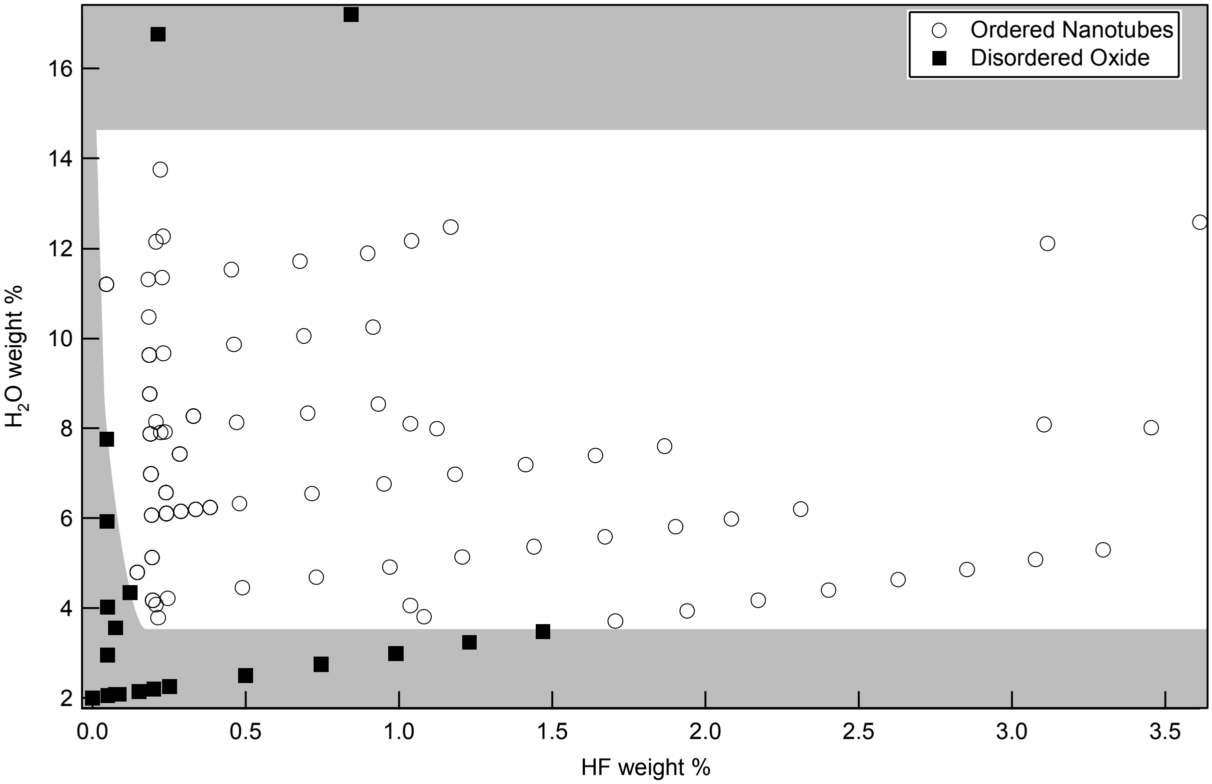

Figure 4.5: Solution phase diagram of nanotube growth. Nanotubes grow between 3.6% H_2O, up to ~16% H_2O where the H_2SO_4 medium is fully deprotonated to HSO_4^-.

equivalent to the fastest observed growth of porous alumina under high field conditions.[17] The tube length saturated quickly in these fast growing tubes, and the maximum observed length after both 20 min and 4 h was 35 μm. TEM comparison of the base of the tube vs. the tip revealed pronounced nanotube wall tapering (Fig. 4.6). When the nanotube was grown for more than 12 h, the substrate etched away entirely. This etching, combined with the nanotube length saturation, wall tapering, and continuous electrochemical current, suggests a competition between the non-specific etching of the nanotubes by HF in solution and the electrochemical growth of the nanotubes. These results compare well with previous observations in TiO_2 nanotubes, where the maximum nanotube lengths were limited to ~4.4 μm in aqueous electrolytes.[10, 87] Beyond the observed tapering of the nanotube walls, we found that the outer diameter of the base of the nanotubes could be controlled by the HF concentration. Higher HF concentrations (0.2 - 2.0%) decreased the outer diameters while the inner diameters remained unchanged. (Fig. 4.7)

We were limited in our ability to test higher water concentrations using HF as a fluorine source, because at high H_2O concentrations the current density exceeded the capacity of the available power supply. By replacing HF with KF in the solution the current density was reduced by ~80%, and we reached higher H_2O concentrations of 16-18% by weight, or in excess of 50% by molarity. Because the molarity of water exceeded the molarity of H_2SO_4, the acid was entirely in the HSO_4^- species, nanotubes did not grow, and only unstructured amorphous oxide was observed. These results strongly suggest the H_2SO_4 species plays a role in the chemistry of Ta_2O_5 nanotube growth.

As the tantalum oxide nanotubes are not in contact with each other at the growth zone, the HCP ordering is unlikely to occur by an expanding oxide mechanism similar to that proposed for porous alumina. We propose an alternate mechanism derived from the electron avalanche model

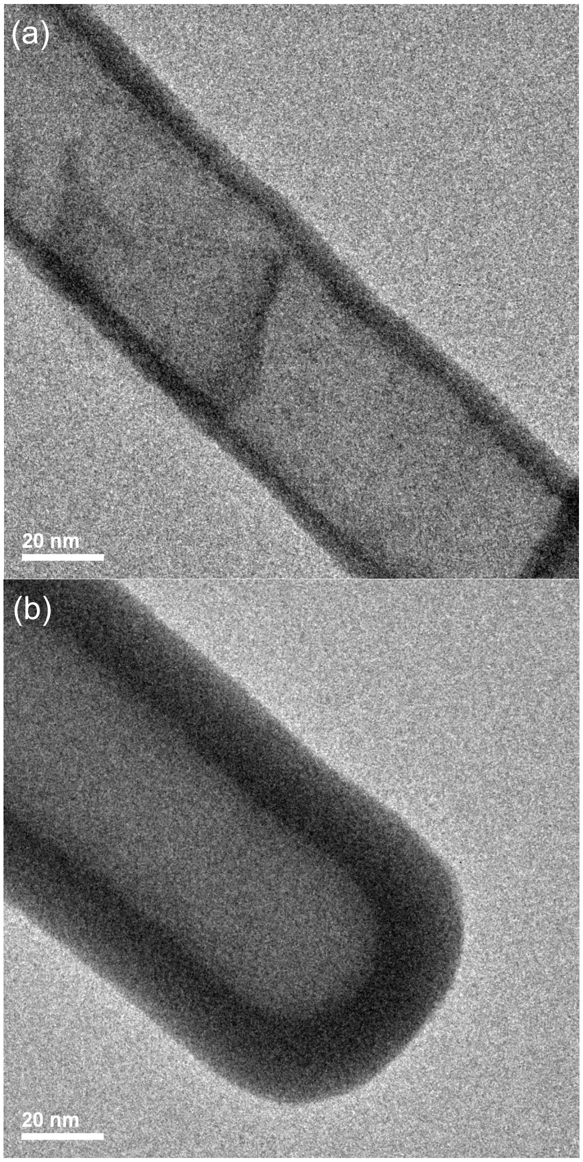

Figure 4.6: TEM images of (a) top and (b) bottom of a 35-µm long Ta_2O_5 nanotube revealing a significant tapering of the nanotube outer diameter over time.

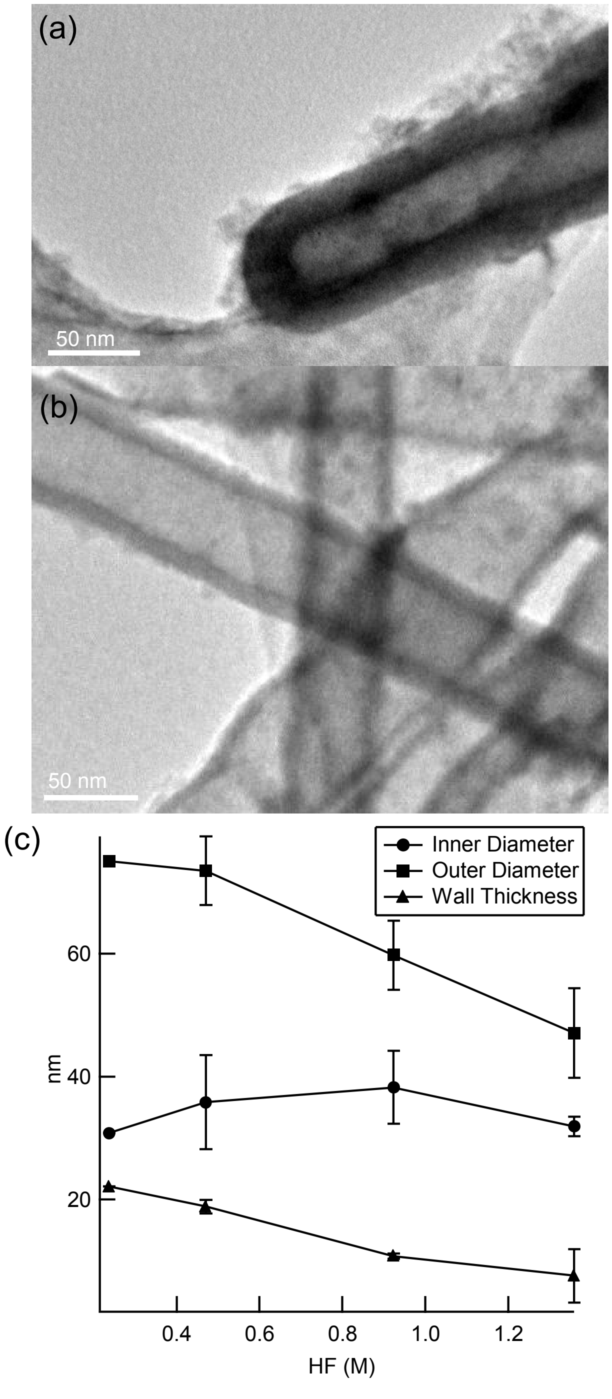

Figure 4.7: TEM images of (a) 0.25% HF grown nanotubes and (b) 1% HF grown nanotubes. The scalebars are 50 nm. The graph in (c) shows the averaged nanotube outer diameter, inner diameter, and wall thickness vs. HF concentration.

of dielectric breakdown.[97] Electrons are liberated from fluorine ions incorporated into the oxide, and these electrons are accelerated through the oxide film toward the tantalum anode by the applied voltage. Through impact ionization, each of these electrons liberates additional electrons from the oxide and generates an electron avalanche which is conducted away by the circuit, leaving a positive space charge in the pore oxide. The electrostatic repulsion of the space charge generated within each pore causes the self-ordering effect. In uniform anodic oxide films dielectric breakdown occurs because at higher fields electron avalanche events occur more frequently, and eventually the overlap of electron avalanches breaks down dielectric oxide by joule heating.[97] Under this model the higher ordering of porous structures anodized near the dielectric breakdown voltage is attributed to the increasing number of electron avalanche events, which increase the magnitude of the space-charge within the pores and thus the electrostatic repulsion. The charge in the oxide will be neutralized periodically as space-charge exceeds the applied bias and current flows in reverse, disrupting continuous nanotube growth as observed in the ridges which decorate the outer nanotube walls (Fig. 4.3(b)). The disorder observed in Ta_2O_5 nanotubes anodized at high voltage can be attributed to dielectric breakdown of the oxide perturbing the applied potential in time.

The same mechanism can explain the formation and ordering of porous aluminum oxide membranes with one addition. The ion mobility of Al^{3+} is higher than that of Ti^{4+} or Ta^{5+}, and horizontal diffusion of Al^{3+} repelled by the positive charge within the pore oxide leads to oxide expansion, filling the interstitial spaces between aluminum oxide nanotubes.[57] This interpretation is supported by the selective dissolution of aluminum oxide between pores,[9] and the equivalent selective dissolution of the outer portion of tantalum oxide nanotubes (Fig. 4.6) which is formed from slower horizontal Ta^{5+} diffusion.

4.4 TaS_2 Inorganic Fullerenes

We have previously applied solid state techniques to chemically transform patterned transition metal and metal oxide nanostructures into their sulfide analogues without substantially altering their morphology.[98-100] Here we apply similar conversion conditions to generate TaS_2 fullerene-like nanotubes from the Ta_2O_5 nanotube template.

Certain polytypes of bulk TaS_2 (2H and 6R) are low temperature Type II superconductors (T_c 0.8 and 2.3 K, respectively) with a layered sheet 2D crystal structure. Bulk 6R-TaS_2 exhibits an incommensurate-commensurate charge density wave (CDW) transition at 100 K, while bulk 2H-TaS_2 exhibits a similar CDW transition at 75 K.[101] Intercalation studies have demonstrated a dramatic increase of T_c up to 9 K, which was attributed to reduced dimensionality of the material as interplane coupling was reduced by increased c-axis spacing.[102] Directly disruption of the CDW by high pressure demonstrated an increase of 2H-TaS_2 T_c to 2.1 K and a CDW T_0 decrease to 70 K at 20 kbar.[103] Previous studies of single-crystalline 20-nm diameter TaS_2 nanowires showed an increase of T_c up to 3.4 K, which was attributed to competing CDW suppression in nanostructures.[104, 105]

Layered inorganic chalcogenides such as WS_2, MoS_2, and TaS_2 have been observed to wrap into concentric tubular structures analogous to multiwalled carbon nanotubes.[106-109] There has been only one report of polydisperse TaS_2 nanotubes (4-15 nm diameters) grown from the decomposition of a TaS_3 precursor. These nanotubes were unstable under an electron beam, and no characterization of the electronic properties was reported.[110] The synthesis of stable, tunable, high quality TaS_2 fullerene materials with a controllable number of walls can allow systematic investigations of how dimensionality affects complex electronic properties like CDW behavior and superconductivity.

4.4.1 TaS_2 Synthesis

Crystalline and amorphous Ta_2O_5 nanotubes of several sizes were converted to TaS_2 layered nanotubes by annealing under H_2S gas. Samples were placed in a 1”-tube furnace, and the temperature was ramped to 625 ^oC at a rate of 2 ^oC/min under H_2S at ~1-5 Torr, held at that temperature for 12 h, and then cooled over 90 min. The resulting product was a black powder. Conversion of amorphous Ta_2O_5 templates produced superior TaS_2 products, while crystalline templates were fragile and yielded short polycrystalline nanotubes. Sulfidization was studied by annealing amorphous and crystalline Ta_2O_5 nanotubes under H_2S between 400 and 900 ^oC.

4.4.2 TaS_2 Materials Characterization

SEM indicated that the original nanotube structure was preserved, and HR-TEM and SAED revealed that the crystalline structure of the tubes was similar to multiwalled inorganic fullerene structures (Fig. 4.8). The SAED pattern showed two sharp dots perpendicular to the tube direction, representing the intertube wall distance. The other scattered dots are all distorted in the direction same direction as the tube walls. The random pattern of the dots indicates multiple chiralities of nanotubes, while the distortion is a product of the tube curvature. The spacing of the a and b axes with respect to the electron beam varies across the nanotube as the curvature affects the angle of beam incidence. This variation translates to the observed distortion in the SAED pattern. GA-PXRD suggested that the TaS_2 nanotubes crystallized in the 2H-TaS_2 polytype.[101] The interwall spacing of 40, 50, 80, and 100-nm nanotubes from the GA-PXRD spectra was 6.03-6.06 Å, which aligned well with the interlayer spacing of 2H-TaS_2 and demonstrated little evidence of lattice strain. XPS characterization showed that TaS_2 tubes

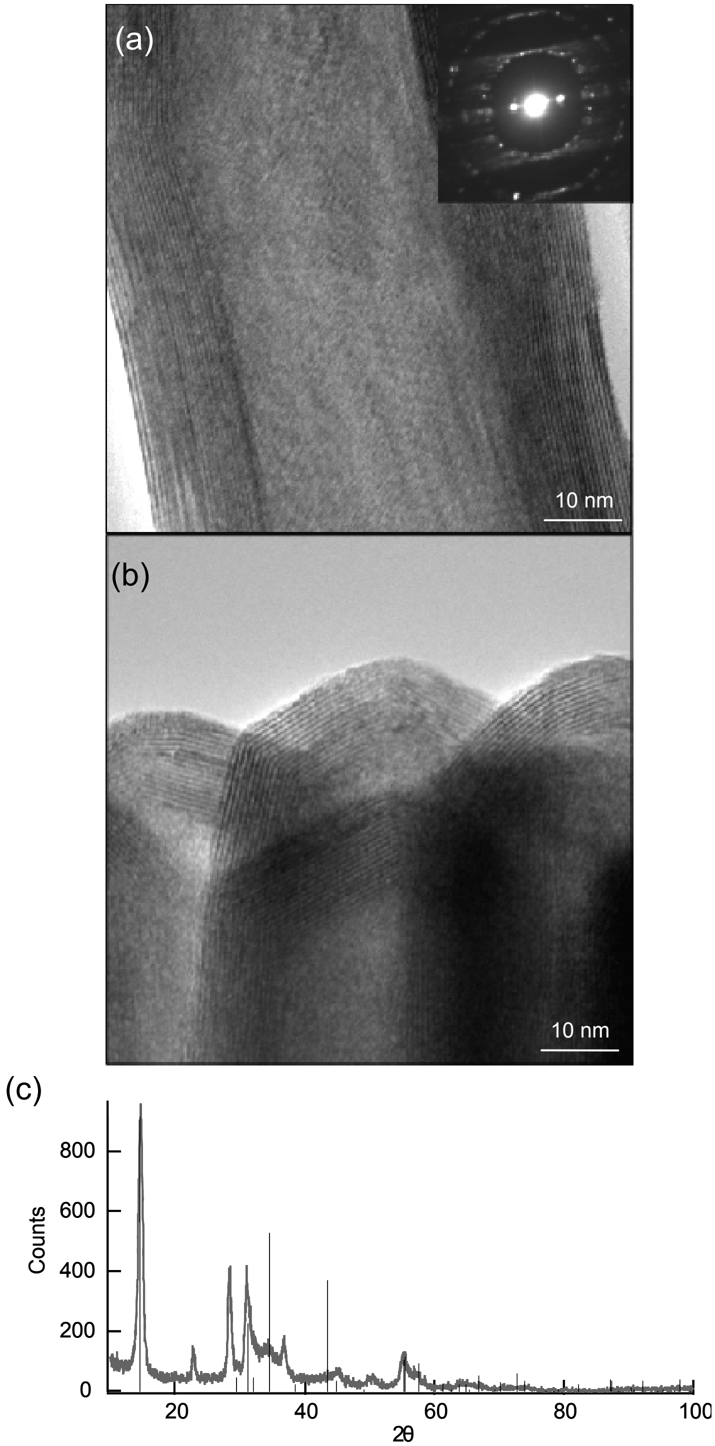

Figure 4.8: TEM images of layered tantalum disulfide nanotube (a) walls and (b) ends. SAED (a, inset) reveals a multilayered fullerene morphology of the structure and multiple chiralities, while (c) PXRD of 2H-TaS_2 nanotubes. The lines represent bulk 2H-TaS_2 peak positions and intensities.

contained some Ta^{5+} ions. Scanning TEM linescan profiles showed no detectable oxygen in the structure of pristine nanotubes.

A superconducting quantum interference device (SQUID) magnetometer was used to measure the temperature-dependent DC magnetic susceptibility of the TaS_2 nanotubes. This technique provided information on the magnetic properties of the TaS_2, which directly relate to superconductivity and CDW behavior.[101] Field cooled DC-magnetization of 40, 50, 80, and 100-nm diameter nanotubes at 5 Oe revealed TaS_2 nanotubes have a T_c around 2.8-3 K, which is 2-2.2 K higher than bulk 2H-TaS_2 and comparable to the T_c of polydisperse 2H-TaS_2 nanowires.[104] Although the proposed mechanism for increased T_c in the nanowires was the suppression of the competing CDW in the nanoscale material, but no direct measurements of CDW transitions were made.[104] Magnetization measurements at 500 Oe revealed a CDW transition around 60 K, which was ~10 K lower than bulk 2H-TaS_2. Bulk 2H-TaS_2 has a superconducting T_c of 0.8 K, while polydisperse 2H-TaS_2 nanowire have a substantially higher T_c of 3.4 K.[101, 104, 105] In the bulk, a 2 K increase in 2H-TaS_2 T_c requires a pressure of ~24 kbar, while a 10 K decrease in CDW T_0 requires a pressure of 53 kbar.[103, 111] As the TaS_2 CDW is entirely suppressed at 43 kbar something else is at work in this experiment. One possible mechanism for this phenomenon is a further reduction of interlayer coupling because of the multi-chiral structure of the nanotubes.

4.6 Summary

Here we report the rapid (1-20 min timescale) anodic self-ordered growth of amorphous tantalum oxide nanotubes in an extremely wide process window. We can achieve independent control over the length, diameter, and wall thickness, in amorphous and crystalline Ta_2O_5 nanotubes. Moreover, these Ta_2O_5 nanotubes function as templates for a

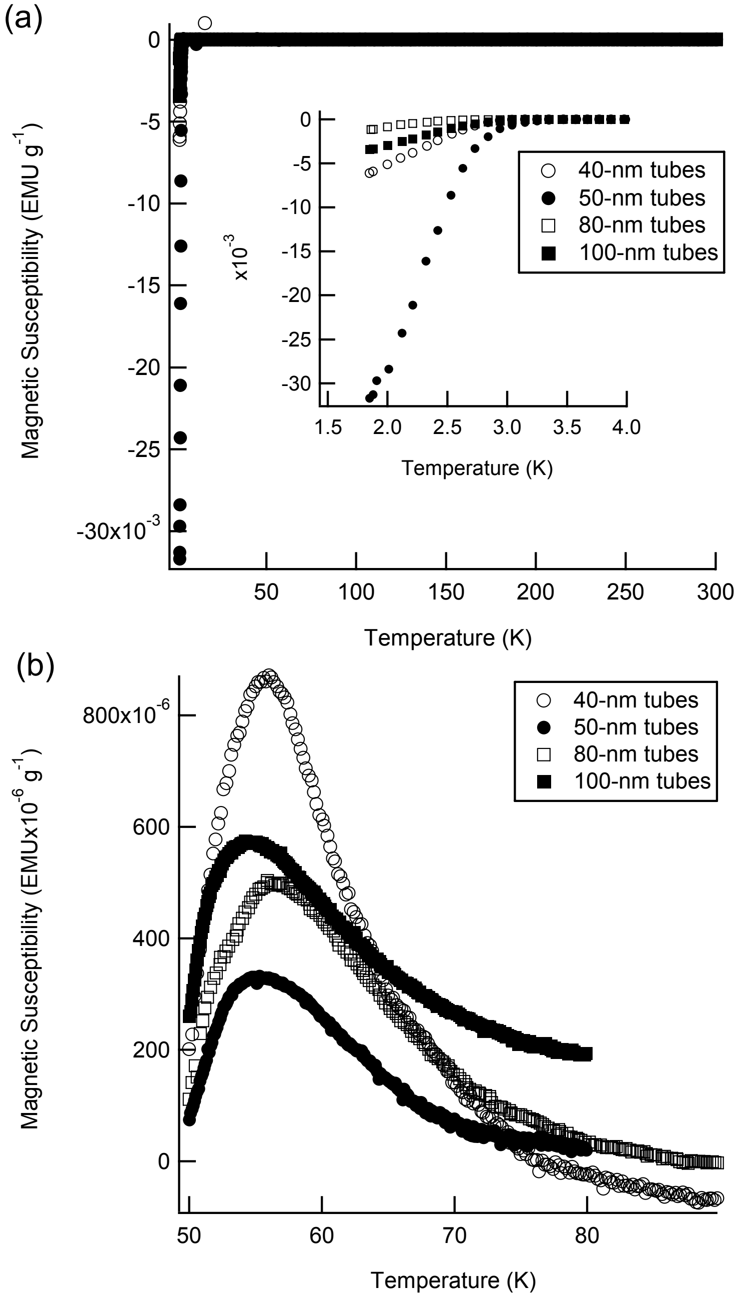

Figure 4.9: TaS_2 magnetic susceptibility (a) under 5 Oe with inset near the superconducting T_c, and (b) under 500 Oe near the 2H-TaS_2 and CDW T_0.

chemical transformation to 2H-TaS_2 nanotubes with an inorganic fullerene structure. DC magnetic susceptibility measurements revealed an increased superconducting T_c and suppressed CDW transitions.

References

1. Binnig, G.; Rohrer, H.; Ch, G.; Weibel, E., Tunneling through a controllable vacuum gap. *Applied Physics Letters* **1982,** 40, (2), 178-180.

2. Amama, P. B.; Maschmann, M. R.; Fisher, T. S.; Sands, T. D., Dendrimer-Templated Fe Nanoparticles for the Growth of Single-Wall Carbon Nanotubes by Plasma-Enhanced CVD. *J. Phys. Chem.* **2006,** 110, (22), 10636-10644.

3. Taubert, A.; Wiesler, U. M.; Mullen, K., Dendrimer-controlled one-pot synthesis of gold nanoparticles with a bimodal size distribution and their self-assembly in the solid state. *Journal of Materials Chemistry* **2003,** 13, (5), 1090-1093.

4. Zhang, Z.; Patel, R. C.; Kothari, R.; Johnson, C. P.; Friberg, S. E.; Aikens, P. A., Stable Silver Clusters and Nanoparticles Prepared in Polyacrylate and Inverse Micellar Solutions. *J. Phys. Chem. B* **2000,** 104, (6), 1176-1182.

5. Lin, X. M.; Sorensen, C. M.; Klabunde, K. J.; Hadjipanayis, G. C., Temperature Dependence of Morphology and Magnetic Properties of Cobalt Nanoparticles Prepared by an Inverse Micelle Technique. *Langmuir* **1998,** 14, (25), 7140-7146.

6. Martin, J. E.; Wilcoxon, J. P.; Odinek, J. G.; Provencio, P. P., Control of the interparticle spacing in gold nanoparticle superlattices. *J. Phys. Chem. B* **2000,** 104, (40), 9475-9486.

7. Cheng, G. X.; Shen, F.; Yang, L. F.; Ma, L. R.; Tang, Y.; Yao, K. D.; Sun, P. C., On properties and structure of the AOT-water-isooctane reverse micellar microreactor for nanoparticles. *Materials Chemistry and Physics* **1998,** 56, (2), 97-101.

8. Odom, T. W.; Thalladi, V. R.; Love, J. C.; Whitesides, G. M., Generation of 30-50 nm Structures Using Easily Fabricated, Composite PDMS Masks. *Journal of the American Chemical Society* **2002,** 124, (41), 12112-12113.

9. Chu, S.-Z.; Wada, K.; Inoue, S.; Isogai, M.; Yasumori, A., Fabrication of Ideally Ordered Nanoporous Alumina Films and Integrated Alumina Nanotubule Arrays by High-Field Anodization. *Advanced Materials* **2005,** 17, (17), 2115-2119.

10. Gong, D.; Grimes, C. A.; Varghese, O. K.; Hu, W.; Singh, R. S.; Chen, Z.; Dickey, E. C., Titanium oxide nanotube arrays prepared by anodic oxidation. *Journal of Materials Research* **2001,** 16, (12), 3331-3334.

11. Masuda, H.; Fukuda, K., Ordered Metal Nanohole Arrays Made by a Two-Step Replication of Honeycomb Structures of Anodic Alumina 10.1126/science.268.5216.1466. *Science* **1995,** 268, (5216), 1466-1468.

12. Masuda, H.; Hasegwa, F.; Ono, S., Self-Ordering of Cell Arrangement of Anodic Porous Alumina Formed in Sulfuric Acid Solution. *Journal of The Electrochemical Society* **1997,** 144, (5), L127-L130.

13. Masuda, H.; Yada, K.; Osaka, A., Self-ordering of cell configuration of anodic porous alumina with large-size pores in phosphoric acid solution. *Japanese Journal of Applied Physics Part 2-Letters* **1998,** 37, (11A), L1340-L1342.

14. Shingubara, S.; Morimoto, K.; Sakaue, H.; Takahagi, T., Self-organization of a porous alumina nanohole array using a sulfuric/oxalic acid mixture as electrolyte. *Electrochemical and Solid State Letters* **2004,** 7, (3), E15-E17.

15. Nielsch, K.; Choi, J.; Schwirn, K.; Wehrspohn, R. B.; Gosele, U., Self-ordering regimes of porous alumina: The 10% porosity rule. *Nano Letters* **2002,** 2, (7), 677-680.

16. Ono, S.; Saito, M.; Asoh, H., Self-Ordering of Anodic Porous Alumina Induced by Local Current Concentration: Burning. *Electrochemical and Solid-State Letters* **2004,** 7, (7), B21-B24.

17. Lee, W.; Ji, R.; Gosele, U.; Nielsch, K., Fast fabrication of long-range ordered porous alumina membranes by hard anodization. *Nat Mater* **2006,** 5, (9), 741-747.

18. Lee, J.; Choi, J.; Lee, J.; Choi, S. K.; Chun, H. D., Electrostatic capacitance of TiO2 nanowires in a porous alumina template. *Nanotechnology* **2005,** 16, 1449-1453.

19. Ikezawa, Y.; Nishimura, K.; Uchida, H.; Inoue, M., Preparation of two-dimensional magneto-photonic crystals of bismus substitute yttrium iron garnet materials. *Journal of Magnetism and Magnetic Materials* **2004,** 272-276, (Part 3), 1690-1691.

20. Piao, Y.; Lim, H.; Chang, J. Y.; Lee, W.-Y.; Kim, H., Nanostructured materials prepared by use of ordered porous alumina membranes. *Electrochimica Acta* **2005,** 50, (15), 2997-3013.

21. Choi, J.; Sauer, G.; Goring, P.; Nielsch, K.; Wehrspohn, R. B.; Gosele, U., Monodisperse metal nanowire arrays on Si by integration of template synthesis with silicon technology. *Journal of Materials Chemistry* **2003,** 13, (5), 1100-1103.

22. Nicewarner-Pena, S. R.; Freeman, R. G.; Reiss, B. D.; He, L.; Pena, D. J.; Walton, I. D.; Cromer, R.; Keating, C. D.; Natan, M. J., Submicrometer Metallic Barcodes. *Science* **2001,** 294, (5540), 137-141.

23. Steinhart, M.; Wendorff, J. H.; Greiner, A.; Wehrspohn, R. B.; Nielsch, K.; Schilling, J.; Choi, J.; Gosele, U., Polymer Nanotubes by Wetting of Ordered Porous Templates. *Science* **2002,** 296, (5575), 1997-.

24. Park, S. J.; Ahn, B. K.; Alegaonkar, P. S.; Shin, H. J.; Yoo, J. B., Fabrication of Porous Al2O3 and TiO2 Thin film hybrid composite using Atomic Layer Deposition and Properties Study. *Sold State Phenomena* **2007,** 124-126, 1273-1276.

25. Hashishin, T.; Tono, Y.; Tamaki, J., Guide Growth of Carbon NAnotube Arrays Using Anodic Porous Alumina with Ni Catalyst. *Jpn. J. Appl. Phys.* **2006,** 45, 333-337.

26. Alivisatos, A. P., Semiconductor clusters, nanocrystals, and quantum dots. *Science* **1996,** 271, (5251), 933-7.

27. Hu, J.; Odom, T. W.; Lieber, C. M., Chemistry and Physics in One Dimension: Synthesis and Properties of Nanowires and Nanotubes. *Accounts of Chemical Research* **1999,** 32, (5), 435-445.

28. Murray, C. B.; Norris, D. J.; Bawendi, M. G., Synthesis and characterization of nearly monodisperse CdE (E = sulfur, selenium, tellurium) semiconductor nanocrystallites. *Journal of the American Chemical Society* **1993,** 115, (19), 8706-15.

29. Puntes, V. F.; Krishnan, K. M.; Alivisatos, A. P., Colloidal nanocrystal shape and size control: The case of cobalt. *Science* **2001,** 291, (5511), 2115-2117.

30. Larsen, G.; Lotero, E.; Marquez, M., Use of Polypropyleneimine Tetrahexacontaamine (DAB-Am-64) Dendrimer as a Single Molecule Template To Produce Mesoporous Silicas. *Chemistry of Materials* **2000,** 12, (6), 1513-1515.

31. Groehn, F.; Bauer, B. J.; Akpalu, Y. A.; Jackson, C. L.; Amis, E. J., Dendrimer Templates for the Formation of Gold Nanoclusters. *Macromolecules* **2000,** 33, (16), 6042-6050.

32. Petit, C.; Pileni, M. P., Synthesis of cadmium sulfide in situ in reverse micelles and in hydrocarbon gels. *Journal of Physical Chemistry* **1988,** 92, (8), 2282-6.

33. Whitney, T. M.; Jiang, J. S.; Searson, P. C.; Chien, C. L., Fabrication and magnetic properties of arrays and metallic nanowires. *Science* **1993,** 261, (5126), 1316-19.

34. Hulteen, J. C.; Martin, C. R., A general template-based method for the preparation of nanomaterials. *Journal of Materials Chemistry* **1997,** 7, (7), 1075-1087.

35. Jackman, R. J.; Duffy, D. C.; Ostuni, E.; Willmore, N. D.; Whitesides, G. M., Fabricating Large Arrays of Microwells with Arbitrary Dimensions and Filling Them Using Discontinuous Dewetting. *Analytical Chemistry* **1998,** 70, (11), 2280-2287.

36. Chan, E. M.; Mathies, R. A.; Alivisatos, A. P., Size-controlled growth of CdSe nanocrystals in microfluidic reactors. *Nano Letters* **2003,** 3, (2), 199-201.

37. Edel, J. B.; Fortt, R.; de Mello, J. C.; de Mello, A. J., Microfluidic routes to the controlled production of nanoparticles. *Chemical Communications* **2002**, (10), 1136-1137.

38. Jensen, K. F., Microreaction engineering - is small better? *Chemical Engineering Science* **2001,** 56, (2), 293-303.

39. Wang, X.; Summers, C. J.; Wang, Z. L., Large-Scale Hexagonal-Patterned Growth of Aligned ZnO Nanorods for Nano-optoelectronics and Nanosensor Arrays. *Nano Letters* **2004,** 4, (3), 423-426.

40. Gan, F. Y.; Shih, I., Thin film transistors with anodic gate dielectrics and chemical bath deposited active layers. *Journal of Vacuum Science & Technology A: Vacuum, Surfaces, and Films* **2002,** 20, (4), 1365-1368.

41. Kenis, P. J. A.; Ismagilov, R. F.; Takayama, S.; Whitesides, G. M.; Li, S.; White, H. S., Fabrication inside Microchannels Using Fluid Flow. *Accounts of Chemical Research* **2000,** 33, (12), 841-847.

42. Qin, D.; Xia, Y.; Xu, B.; Yang, H.; Zhu, C.; Whitesides, G. M., Fabrication of ordered two-dimensional arrays of micro- and nanoparticles using patterned self-assembled monolayers as templates. *Advanced Materials* **1999,** 11, (17), 1433-1437.

43. Grzybowski, B. A.; Haag, R.; Bowden, N.; Whitesides, G. M., Generation of Micrometer-Sized Patterns for Microanalytical Applications Using a Laser Direct-Write Method and Microcontact Printing. *Analytical Chemistry* **1998,** 70, (22), 4645-4652.

44. Thalladi, V. R.; Whitesides, G. M., Crystals of Crystals: Fabrication of Encapsulated and Ordered Two-Dimensional Arrays of Microcrystals. *Journal of the American Chemical Society* **2002,** 124, (14), 3520-3521.

45. Aizenberg, J.; Black, A. J.; Whitesides, G. M., Oriented Growth of Calcite Controlled by Self-Assembled Monolayers of Functionalized Alkanethiols Supported on Gold and Silver. *Journal of the American Chemical Society* **1999,** 121, (18), 4500-4509.

46. Chou, S. Y.; Keimel, C.; Gu, J., Ultrafast and direct imprint of nanostructures in silicon. *Nature* **2002,** 417, (6891), 835-837.

47. Glasgov, V. M.; Chizhevaskaya, S. N.; Glagoleva, N. N., *Liquid Semiconductors*. Plenum Press: Plenum, NY, 1969; p 362.

48. Langen, M.; Hibiya, T.; Eguchi, M.; Egry, I., Measurement of the density and the thermal expansion coefficient of molten silicon using electromagnetic levitation. *Journal of Crystal Growth* **1998,** 186, (4), 550-556.

49. Haes, A. J.; Van Duyne, R. P., A nanoscale optical biosensor: Sensitivity and selectivity of an approach based on the localized surface plasmon resonance spectroscopy of triangular silver nanoparticles. *Journal of the American Chemical Society* **2002,** 124, (35), 10596-10604.

50. Stober, W.; Fink, A.; Bohn, E., Controlled growth of monodisperse silica spheres in the micron size range. *Journal of Colloid and Interface Science* **1968,** 26, (1), 62-69.

51. Bogush, G. H.; Tracy, M. A.; Zukoski, C. F., Preparation of monodisperse silica particles: Control of size and mass fraction. *Journal of Non-Crystalline Solids* **1988,** 104, (1), 95-106.

52. Wostyn, K.; Zhao, Y.; Yee, B.; Clays, K.; Persoons, A.; de Schaetzen, G.; Hellemans, L., Optical properties and orientation of arrays of polystyrene spheres deposited using convective self-assembly. *The Journal of Chemical Physics* **2003,** 118, (23), 10752-10757.

53. Deegan, R. D.; Bakajin, O.; Dupont, T. F.; Huber, G.; Nagel, S. R.; Witten, T. A., Capillary flow as the cause of ring stains from dried liquid drops. *Nature* **1997,** 389, (6653), 827-829.

54. Huang, J.; Kim, F.; Tao, A. R.; Connor, S.; Yang, P., Spontaneous formation of nanoparticle stripe patterns through dewetting. *Nat Mater* **2005,** 4, (12), 896-900.

55. Kim, E.; Xia, Y.; Whitesides, G. M., Two- and three-dimensional crystallization of polymeric microspheres by micromolding in capillaries. *Advanced Materials* **1996,** 8, (3), 245-247.

56. Xia, Y.; McClelland, J. J.; Gupta, R.; Qin, D.; Zhao, X. M.; Sohn, L. L.; Celotta, R. J.; Whitesides, G. M., Replica molding using polymeric materials: A practical step toward nanomanufacturing. *Advanced Materials* **1997,** 9, (2), 147-149.

57. *CRC Handbook of Chemistry and Physics*. 77th ed.; CRC Press: Boca Raton, FL, 1996.

58. Barton, J. E.; Odom, T. W., Mass-Limited Growth in Zeptoliter Beakers: A General Approach for the Synthesis of Nanocrystals. *Nano Letters* **2004,** 4, (8), 1525-1528.

59. Gudiksen, M. S.; Lauhon, U. J.; Wang, J.; Smith, D. C.; Lieber, C. M., Growth of nanowire superlattice structures for nanoscale photonics and electronics. *Nature* **2002,** 415, (6872), 617-620.

60. Hata, K.; Futaba, D. N.; Mizuno, K.; Namai, T.; Yumura, M.; Iijima, S., Water-Assisted Highly Efficient Synthesis of Impurity-Free Single-Walled Carbon Nanotubes. *Science* **2004,** 306, (5700), 1362-1364.

61. Mohapatra, S. K.; Misra, M.; Mahajan, V. K.; Raja, K. S., Design of a Highly Efficient Photoelectrolytic Cell for Hydrogen Generation by Water Splitting: Application of TiO2-xCx Nanotubes as a Photoanode and Pt/TiO2 Nanotubes as a Cathode. *J. Phys. Chem. C* **2007,** 111, (24), 8677-8685.

62. Liu, D.; Chen, J.; Deng, W.; Zhou, H.; Kuang, Y., Simple catalyst for the direct growth of carbon nanotubes onto substrate by chemical vapor deposition. *Materials Letters* **2004,** 58, (22-23), 2764-2767.

63. Zheng, L. X.; O'Connell, M. J.; Doorn, S. K.; Liao, X. Z.; Zhao, Y. H.; Akhadov, E. A.; Hoffbauer, M. A.; Roop, B. J.; Jia, Q. X.; Dye, R. C.; Peterson, D. E.; Huang, S. M.; Liu, J.; Zhu, Y. T., Ultralong single-wall carbon nanotubes. *Nat Mater* **2004,** 3, (10), 673-676.

64. Kordás, K.; Pap, A. E.; Vähäkangas, J.; Uusimäki, A.; Leppävuori, S., Carbon nanotube synthesis on oxidized porous silicon. *Applied Surface Science* **2005,** 252, (5), 1471-1475.

65. Futaba, D. N.; Hata, K.; Namai, T.; Yamada, T.; Mizuno, K.; Hayamizu, Y.; Yumura, M.; Iijima, S., 84% Catalyst Activity of Water-Assisted Growth of Single Walled Carbon Nanotube Forest Characterization by a Statistical and Macroscopic Approach. *J. Phys. Chem. B* **2006,** 110, (15), 8035-8038.

66. El-Sayed, H.; Singh, S.; Greiner, M. T.; Kruse, P., Formation of Highly Ordered Arrays of Dimples on Tantalum at the Nanoscale. *Nano Lett.* **2006,** 6, (12), 2995-2999.

67. Choi, J.; Wehrspohn, R. B.; Gösele, U., Mechanism of guided self-organization producing quasi-monodomain porous alumina. *Electrochimica Acta* **2005,** 50, (13), 2591-2595.

68. Singh, S.; Greiner, M. T.; Kruse, P., Robust Inorganic Membranes from Detachable Ultrathin Tantalum Oxide Films. *Nano Lett.* **2007,** 7, (9), 2676-2683.

69. El-Sayed, H.; Singh, S.; Kruse, P., Formation of Dimpled Tantalum Surfaces from Electropolishing. *Journal of The Electrochemical Society* **2007,** 154, (12), C728-C732.

70. DePalma, R.; Laureyn, W.; Frederix, F.; Bonroy, K.; Pireaux, J. J.; Borghs, G.; Maes, G., Formation of Dense Self-assembled Monolayers of (n-Decyl)trichlorosilanes on Ta/Ta2O5. *Langmuir* **2007,** 23, (2), 443-451.

71. Keller, F.; Hunter, M. S.; Robinson, D. L., Structural Features of Oxide Coatings on Aluminum. *Journal of The Electrochemical Society* **1953,** 100, 411-419.

72. Li, A. P.; Muller, F.; Birner, A.; Nielsch, K.; Gosele, U., Hexagonal pore arrays with a 50--420 nm interpore distance formed by self-organization in anodic alumina. *Journal of Applied Physics* **1998,** 84, (11), 6023-6026.

73. Li, F.; Zhang, L.; Metzger, R. M., On the Growth of Highly Ordered Pores in Anodized Aluminum Oxide. *Chem. Mater.* **1998,** 10, (9), 2470-2480.

74. Jessensky, O.; Muller, F.; Gosele, U., Self-organized formation of hexagonal pore arrays in anodic alumina. *Applied Physics Letters* **1998,** 72, (10), 1173-1175.

75. Tsuchiya, H.; Macak, J. M.; Ghicov, A.; Taveira, L.; Schmuki, P., Self-organized porous TiO_2 and ZrO_2 produced by anodization. *Corrosion Science* **2005,** 47, (12), 3324-3335.

76. Tsuchiya, H.; Schmuki, P., Thick self-organized porous zirconium oxide formed in H2SO4/NH4F electrolytes. *Electrochemistry Communications* **2004,** 6, (11), 1131-1134.

77. Tsuchiya, H.; Macak, Jan M.; Sieber, I.; Schmuki, P., Self-Organized High-Aspect-Ratio Nanoporous Zirconium Oxides Prepared by Electrochemical Anodization. *Small* **2005,** 1, (7), 722-725.

78. Tsuchiya, H.; Schmuki, P., Self-organized high aspect ratio porous hafnium oxide prepared by electrochemical anodization. *Electrochemistry Communications* **2005,** 7, (1), 49-52.

79. Sieber, I.; Hildebrand, H.; Friedrich, A.; Schmuki, P., Formation of self-organized niobium porous oxide on niobium. *Electrochemistry Communications* **2005,** 7, (1), 97-100.

80. Tsuchiya, H.; Macak, J. M.; Sieber, I.; Taveira, L.; Ghicov, A.; Sirotna, K.; Schmuki, P., Self-organized porous WO_3 formed in NaF electrolytes. *Electrochemistry Communications* **2005,** 7, (3), 295-298.

81. Lee, W.-J.; Smyrl, W. H., Zirconium Oxide Nanotubes Synthesized via Direct Electrochemical Anodization. *Electrochemical and Solid-State Letters* **2005,** 8, (3), B7-B9.

82. Paulose, M.; Shankar, K.; Yoriya, S.; Prakasam, H. E.; Varghese, O. K.; Mor, G. K.; Latempa, T. A.; Fitzgerald, A.; Grimes, C. A., Anodic Growth of Highly Ordered TiO_2 Nanotube Arrays to 134 um in Length. *J. Phys. Chem. B* **2006,** 110, (33), 16179-16184.

83. Macak, Jan M.; Zlamal, M.; Krysa, J.; Schmuki, P., Self-Organized TiO_2 Nanotube Layers as Highly Efficient Photocatalysts. *Small* **2007,** 3, (2), 300-304.

84. Macak, J. M.; Aldabergerova, S.; Ghicov, A.; Schmuki, P., Smooth anodic TiO_2 nanotubes: annealing and structure. *physica status solidi (a)* **2006,** 203, (10), R67-R69.

85. Varghese, O. K.; Paulose, M.; Shankar, K.; Mor, G. K.; Grimes, C. A., Water-Photolysis Properties of Micron-Length Highly-Ordered Titania Nanotube-Arrays. *Journal of Nanoscience and Nanotechnology* **2005,** 5, 1158-1165.

86. Macak, J. M.; Tsuchiya, H.; Taveira, L.; Aldabergerova, S.; Schmuki, P., Smooth Anodic TiO_2 Nanotubes. *Angew Chem. Int. Ed.* **2005,** 44, (45), 7463-7465.

87. Cai, Q.; Paulose, M.; Varghese, O. K.; Grimes, C. A., The effect of electrolyte composition on the fabrication of self-ordered titanium oxide nanotube arrays by anodic oxidation. *J. Mater. Res.* **2005,** 20, (1), 230-236.

88. Zeng, W.; Eisenbraun, E.; Frisch, H.; Sullivan, J. J.; Kaloyeros, A. E.; Martgalit, J.; Beck, K., CVD of Tantalum Oxide Dielectric Thin Films for Nanoscale Device Applications. *Journal of The Electrochemical Society* **2004,** 151, (8), F172-F177.

89. Maiti, C. K.; Samanta, S. K.; Chatterjee, S.; Dalapati, G. K.; Bera, L. K., Gate Dielectrics on strained-Si/SiGe heterolayers. *Solid-State Electronics* **2004,** 40, 1369-1389.

90. Lu, J. Hafnium-Doped Tantalum Oxide High-K Gate Dielectric Films for Future CMOS Technology. Texas A&M, College Station, TX, 2005.

91. Murase, T.; Irie, H.; Hashimoto, K., Visible Light Sensitive Photocatalysts, Nitrogen-Doped Ta_2O_5 Powders. *J. Phys. Chem. B* **2004,** 108, 15803-15807.

92. Frenning, G.; Nilsson, M.; Westlinder, J.; Niklasson, G. A.; Mattsson, M. S., Dielectric and Li transport properties of electron conducting and non-conducting sputtered amorphous Ta2O5 films. *Electrochimica Acta* **2001,** 46, (13-14), 2041-2046.

93. Whittingham, M. S., Lithium Batteries and Cathode Materials. *Chem. Rev.* **2004,** 104, 4271-4301.

94. Jinyoung, K.; Jaephil, C., Rate Characteristics of Anatase TiO[sub 2] Nanotubes and Nanorods for Lithium Battery Anode Materials at Room Temperature. *J. Electrochem. Soc.* **2007,** 154, (6), A542-A546.

95. Chen, M. H.; Huang, Z. C.; Wu, G. T.; Zhu, G. M.; You, J. K.; Lin, Z. G., Synthesis and characterization of SnO-carbon nanotube composite as anode material for lithium-ion batteries. *Materials Research Bulletin* **2003,** 38, (5), 831-836.

96. Kazanskii, V. B.; Solkan, V. N., Solvation of Protons in Anhydrous H2SO4 as the Main Factor Determining Its Superacidic Properties. *Kinetics and Catalysis* **2000,** 41, (1), 38-41.

97. Albella, J. M.; Montero, I.; Martinez-Duart, J. M.; Parkhutik, V., Dielectric breakdown processes in anodic Ta2O5 and related oxides. *Journal of Materials Science* **1991,** 26, (13), 3422-3432.

98. Stender, C. L.; Odom, T. W., Chemical nanofabrication: A general route to surface-patterned and free-standing transition metal chalcogenide nanostructures. *Journal of Materials Chemistry* **2007,** 17, (19), 1866-1869.

99. Stender, C. L.; Greyson, E. C.; Babayan, Y.; Odom, T. W., Patterned MoS2 nanostructures over centimeter-square areas. *Advanced Materials* **2005,** 17, (23), 2837-2841.

100. Henzie, J.; Barton, J. E.; Stender, C. L.; Odom, T. W., Large-Area Nanoscale Patterning: Chemistry Meets Fabrication. *Accounts of Chemical Research* **2006,** 39, (4), 249-257.

101. Figueroa, E.; Kuo, Y. K.; Olinger, A.; Lloyd, M. A.; Bastin, L. D.; Petrotsatos, S.; Chen, Q.; Dobbs, B.; Dev, S.; Selegue, J. P.; Delong, L. E.; Brock, C. P.; Brill, J. W., Physical-Properties of 6r-Tas2. *Journal of Solid State Chemistry* **1995,** 114, (2), 486-490.

102. Vicent, J. L.; Hillenius, S. J.; Coleman, R. V., Critical-Field Enhancement and Reduced Dimensionality in Superconducting Layer Compounds. *Physical Review Letters* **1980,** 44, (13), 892.

103. Friend, R. H.; Jerome, D.; Frindt, R. F.; Grant, A. J.; Yoffe, A. D., Electrical conductivity and charge density wave formation in $4H_b$ TaS_2 under pressure. *J. Phys. C: Solid State Phys.* **1977,** 10, 1013-1025.

104. Dunnill, C. W.; Edwards, H. K.; Brown, P. D.; Gregory, D. H., Single-Step Synthesis and Surface-Assisted Growth of Superconducting TaS_2 Nanowires. *Angewandte Chemie* **2006,** 118, (42), 7218-7221.

105. Wu, X.; Tao, Y.; Hu, T.; Song, Y.; Hu, Z.; Zhu, J.; Dong, L., Tantalum disulfide nanobelts: preparation, superconductivity and field emission. *Nanotechnology* **2006,** 17, (1), 201.

106. Tenne, R., Inorganic nanotubes and fullerene-like nanoparticles. *Nature Nanotechnology* **2006,** 1, (2), 103-111.

107. Enyashin, A. N.; Gemming, S.; Bar-Sadan, M.; Popovitz-Biro, R.; Hong, S. Y.; Prior, Y.; Tenne, R.; Seifert, G., Structure and stability of molybdenum sulfide fullerenes. *Angewandte Chemie-International Edition* **2007,** 46, (4), 623-627.

108. Brown, S.; Musfeldt, J. L.; Mihut, I.; Betts, J. B.; Migliori, A.; Zak, A.; Tenne, R., Bulk vs nanoscale WS2: Finite size effects and solid-state lubrication. *Nano Letters* **2007,** 7, (8), 2365-2369.

109. Schuffenhauer, C.; Parkinson, B. A.; Jin-Phillipp, N. Y.; Joly-Pottuz, L.; Martin, J. M.; Popovitz-Biro, R.; Tenne, R., Synthesis of fullerene-like tantalum disulfide nanoparticles by a gas-phase reaction and laser ablation. *Small* **2005,** 1, (11), 1100-1109.

110. Nath, M.; Rao, C. N. R., New Metal Disulfide Nanotubes. *J. Am. Chem. Soc.* **2001,** 123, (20), 4841-4842.

111. Smith, T. F.; Shelton, R. N.; Schwall, R. E., Superconductivity of $TaS_{2-x}Se_x$ layer compounds at high pressure. *J. Phys. F: Metal Phys.* **1975,** 5, 1713-1725.

Appendix: Protocols

I. Silicon Nanowells

1. *Prepare silicon wafer*

   1.1. HF Etch surface oxide

      1.1.1. This step removes surface oxide and improves the fidelity of embossing.

   1.2. Expose to oxygen plasma to render hydrophilic

      1.2.1. This step renders the surface evenly hydrophilic in order to distribute the spheres across the surface

   1.3. Disperse 100-nm silica microspheres onto wafer out of 200-nm pore diameter syringe filter.

      1.3.1. The filter removes sphere aggregates from the solution. Aggregates can nucleate larger irregularities in the resulting film.

   1.4. Tilt wafer to evenly distribute sphere suspension across the surface.

   1.5. Place wet wafer into a petri dish, cover, and elevate one end of the petri dish ~1cm. Leave for ~3-12 hours.

      1.5.1. This angle ensures the suspension dries from the top down, ensuring a constant reservoir of spheres as the suspension dries. If you just dry the wafer flat, most of the spheres deposit around the edges in a disordered mess, and the center often has few or no spheres. By tilting the substrate, you get larger areas of uniform depth. It is easy to tell if the thickness is uniform. There will be distinct color changes when the material goes from, for example, five layers of spheres to six. Brown is one layer. Every other ordered area is red, green, or blue, depending on the thickness. White is typically irregular and over deposited, and should not be used for embossing.

1.6. Dice the substrate into ~1cm square chips. Ideally dice each chip a single color. This supplies a uniform thickness of microspheres.

2. Embossing

2.1. Compress the sphere coated silicon chip against a mechanically robust window of UV grade fused silica.

2.1.1. Good mechanical contact can be observed directly. If the substrate is in poor contact, you will be able to observe a rainbow fringe when you look through the window. This fringe is the interference contrast from the varying thickness of air between the window and the substrate. Compress the chips together until the rainbow vanishes.

2.1.2. This compression can shatter the fused silica windows. I have found that layering three or four clean windows reduces waste by increasing the mechanical strength of the window.

2.2. Impact a ~3x3 mm 200-300 mJ (2-3 J/cm^2) 248-nm excimer beam pulse on the substrate. This energy density is achieved approximately 16 cm from the final spherical lens if using the original optical line. Wear a lab coat, gloves, and the orange goggles.

2.2.1. The laser light can damage your eyes and your skin. If you are wearing the goggles you should see the substrate flash green where the laser hits. This green flash is the fluorescence of the silica spheres.

2.2.2. If necessary, move the substrate and allow the next pulse to hit another area of the substrate. Do not allow the laser beam to impact an area more than once.

2.3. Remove the substrate and clean the window with a clean fiber free towel in order to remove residual debris.

2.3.1. This allows the window to be used easily for the next substrate.

2.3.2. Don't expect to get all the debris off.

2.4. Etch the substrate in HF.

2.4.1. This selectively removes the silica spheres. There is no need to time this reaction. Make sure it runs for at least two minutes, but you cannot over etch it.

3. Modify silicon surface chemistry by silanization

3.1. Use preferred silanization technique.

3.1.1. For 1,1,2,2 tetrahydroperfluorooctadecyltrichlorsilane, subject silicon to oxygen plasma for 30 s, then place in desiccator with 1-2 drops of fluorosilane and place under house vacuum for 2 hours. Heat the substrate to 110 ^{o}C on a hot plate for 20 min to enhance siloxane cross-linking and film stability.

3.1.2. For octadecyltrichlorosilane, oxygen plasma etch the silicon for 30 s, then place in a desiccator with 1-2 drops of octadecyltrichlorosilane and place under house vacuum for 12-24 hours. Heat the substrate to 110 ^{o}C on a hot plate for 20 min to enhance siloxane cross-linking and film stability.

3.2. Rinse with isopropanol.

4. Growing nanoparticles

4.1. Make a solution of an appropriate precursor material.

4.1.1. Metal chlorides make good precursors because they are typically highly soluble high melting point materials, but avoid using metal chlorides with fluorocarbon surface chemistry. Non-specific binding between metal chlorides and fluorocarbon was often observed. This may be due to a fluorine carbon exchange reaction.

4.2. Dewet material. Suspend substrate in solution vertically, and withdraw at ~10-50 microns/second. This is most easily accomplished with a syringe pump.

5. *Reacting nanoparticles.*

5.1. For metal nanoparticles, hydrogen reduce in the tube furnace. Place substrate in the tube furnace and heat under hydrogen to ~80-90% of the precursor melting point at 10°C/min. Soak under hydrogen for ~30 min, then oven cool to room temperature.

5.2. You can also use extremely fast solvent based chemical reactions. You need to ensure that the precursor won't dissolve into solution while you are trying to react it. This is done either by using a solvent system in which your precursor is insoluble, or by using extremely fast reactions. For example, cadmium acetate plus sodium sulfide is sufficiently rapid to avoid precursor nanoparticle dissolution.

6. *Characterize nanoparticles*

6.1. AFM, SEM, and XPS can characterize nanoparticles in situ.

6.2. For TEM, sonicate the substrate (use the probe sonicator) in a small volume of liquid to disperse some of the nanoparticles. The solution can then be used to prepare a TEM grid for high resolution nanoparticle characterization.

II. Tantalum Oxide Nanowells

1. *Electropolish a tantalum film*

1.1. Make a 9:1 H2SO4:48%HF solution. Hook a tantalum film to the + terminal of a DC power supply. Hook a Pt or Pd wire to the – terminal. Place both electrodes in solution and apply a 6V potential for 20 min.

   1.2. This flattens the tantalum film, ensuring a more uniform growth of nanowells in the next step. Ideally the resulting tantalum film will have a mirror polish. If not, repeat until film is very smooth.

2. *Grow initial nanotubes*

2.1. Make up a tantalum electroetch solution. 50 mL of H_2SO_4, and between 0.5-10 mL of 48% HF. Apply potential between electrodes 10-90 volts for 20 min.

   2.2. This grows tantalum oxide nanotubes. Higher HF concentrations grow tubes with thinner walls. Voltage determines nanotube spacing and ultimate nanowell size.

3. *Sonicate tubes off substrate.*

   3.1. This leaves behind a shallow nanowell substrate. These wells are too shallow to dewet into.

4. *Secondary electroetch*

4.1. Make up solution: 50 mL H_2SO_4, 400 µL 48% HF, 2 mL H_2O and heat to 60 ^oC. Immerse electrodes and apply same voltage as before for 0.5-1.5 s.

   4.2. These conditions are optimized for growing 85-nm wells at 30 V. Different voltages may require reoptimization.

   4.3. This step grows very short (~25 nm) nanotubes in the nanowells formed above. These short tubes act as nanowells and can grow nanoparticles.

5. *Surface modification*

5.1. Tantalum oxide nanowells can be modified with silane chemistry.

5.2. Soak the substrate in a room temperature 4:1:1 $H_2O:NH_3OH:H_2O_2$ solution for five s.

5.3. Then place in a desiccator with 1-2 droplets of a volatile silane and leave under house vacuum for 2-24 hours, depending on the silane.

  5.3.1. Octadecyltrichlorosilane needs 12-24 hours. Heat on a hotplate at 110 °C for 20 min to enhance siloxane crosslinking and stabilize the film.

6. *Growing nanoparticles*

  6.1. Make a solution of an appropriate precursor material.

    6.1.1. Metal chlorides make good precursors, but avoid using metal chlorides with fluorocarbon surface chemistry.

  6.2. Dewet material.

  6.2.1. Suspend substrate in solution vertically, and withdraw at ~10-50 microns/second. This is most easily accomplished with a syringe pump.

7. *Reacting nanoparticles.*

  7.1. For metal nanoparticles, hydrogen reduce in the tube furnace.

  7.1.1. Place substrate in the tube furnace and heat under hydrogen to ~80-90% of the precursor melting point at 10°C/min.

  7.1.2. Soak under hydrogen for ~30 min, then oven cool to room temperature.

  7.2. You can also use extremely fast solvent based chemical reactions. You need to ensure that the precursor won't dissolve into solution while you are trying to react it. This is done either by using a solvent system in which your precursor is insoluble, or by using extremely fast reactions. For example, cadmium acetate plus sodium sulfide is sufficiently rapid to avoid nanoparticle dissolution.

  7.3. Repeat the dewetting and reaction steps to add new material to the nanowell.

8. *Characterize nanoparticles*

8.1. AFM, SEM, and XPS can characterize nanoparticles in situ.

8.2. For TEM, sonicate the substrate (use the probe sonicator) in a small volume of liquid to shatter some of the film. This places nanowells into suspension.

8.2.1. The suspension can then be used to prepare a TEM grid for high resolution nanoparticle characterization.

8.2.2. The tantalum oxide nanowells have high Z contrast, so it is very difficult to observe low atomic number crystals.

III. Tantalum Oxide Nanotubes

1. *Electropolish a tantalum film.*

1.1. Make a 9:1 H2SO4:48%HF solution. Hook a tantalum film to the + terminal of a DC power supply.

1.2. Hook a Pt or Pd wire to the – terminal. Place both terminal in solution and apply a 6V potential for 20 min.

1.3. This makes the film flat on the micron scale, and provides a more uniform surface for tube growth.

2. *Grow nanotubes.*

2.1. Create a solution of 0.5-10 mL of 48% HF in 50 mL of H_2SO_4. 0-10 mL of H_2O can also be added.

2.2. Apply a potential between 15-35 V between 1-1000 min. Growth rates are initially quite high, then tapers off over longer periods of time.

2.2.1. Increasing water concentration increases the growth rate substantially. This is due either to increased solution conductivity, or increased supply of oxygen reactants.

2.2.2. Voltage controls the spacing between the tubes, and the inner diameter of the tubes.

2.2.3. HF concentration controls the outer diameter. Increasing HF concentration decreases the outer diameter.

3. *Wash nanotubes.* Nanotubes are very loosely bound to the substrate.

3.1. Tube collection

3.1.1. Immerse H_2SO_4 laden substrate in a beaker of rinse water and sonicate.

3.1.2. Then vacuum filter and rinse to collect the material.

3.2. For retaining ordered tubes on the substrate,

3.2.1. Carefully rinse in beakers of standing water. Experiment with alternate solvents, such as isopropanol or ethanol. This is difficult, particularly with long tubes.

4. *Conversion of amorphous tantalum oxide nanotubes.*

4.1. Nanotubes can be crystallized by annealing in air or oxygen to 750°C for 12 hours.

4.2. Nanotubes can be converted to multiwalled inorganic nanotubes by annealing under 100% H_2S for 12 hours at 625 °C for 2H-TaS_2, or 700 °C for 6R-TaS_2.

IV. Water enhanced carbon nanotubes

1. *Generate a catalyst covered substrate.* Some possibilities below

1.1. Use nanowell substrates to grow separate catalyst particles.

1.1.1. Be sure to use oxidized silicon nanowells with hydrocarbon silanes, as raw silicon and fluorocarbons both poison catalysts.

1.1.2. Use metal nanoparticles. Iron and nickel work well. This gives separated catalysts, ideal for characterizing the effects of water on catalyst activity. Most carbon nanotube growth uses only 1-2 percent of the catalyst material.

2. *Heat substrate to 650-900°C under inert atmosphere.* Argon, helium, and nitrogen work.

2.1. Add a small percent hydrogen to eliminate any oxygen due to leakage.

2.2. This works best over 700°C. 1000-2000 sccm inert gas. 10 sccm H_2.

3. Add water by bubbling inert gas through a water bubbler.

3.1. Water is a weak oxidizing and reducing agent, selectively attacking amorphous carbon which builds up around catalyst particles.

3.2. Maintain a water concentration between 100-300 ppm. -54°F to -26°F or -48°C to -32.2°C dewpoint.

3.2.1. 1-2 sccm flow through bubbler.

3.2.1.1. This flow rate puts a bubble through the bubbler approximately once every five to ten s. While the RH monitor reads this a stable H_2O vapor pressure, it is more likely to put in pulses of higher humidity which may disrupt the nanotube growth.

3.2.2. $\text{ppm} = 3171.2e^{0.0762(\text{Dewpoint in Fahrenheit})}$

3.3. To avoid the H_2O vapor pulses during growth, first pulse a great deal of water through the system, then shut it off.

3.3.1. This will raise the water concentration well above 300 ppm, to the point where water oxidizes the nanotubes.

4. *Turn on carbon source.*
    - 4.1. 100-200 sccm of Ethylene or acetylene work well. Leave on 10 min.
        - 4.1.1. Over time the water concentration falls off, eventually reaching the window of nanotube growth. This procedure works with a total gas flow around 2000 sccm, in which case the vapor pressure typically stabilizes around 50 ppm H_2O.
5. *Turn off ethylene, and cool under inert atmosphere.*
6. *Characterize by SEM and TEM.*

V. Mass-Limited Chemical Gradients

1. *PDMS microwell substrate*
    - 1.1. Spin coat a positive tone photoresist like Shipley 1805 onto a 3.5” silicon wafer
    - 1.2. Expose and develop a pattern of micron scale dots to generate pillars in the photoresist.
    - 1.3. Place 1-2 drops of 1,1,2,2 tetrahydroperfluorooctadecyltrichlorosilane into a vial. Place the vial and the substrate into a desiccators and leave under house vacuum for 2 hours.
        - 1.3.1. This reduces the surface energy of the pattern and makes removal of the final PDMS substrate easier, as well as extending the life of the master.
    - 1.4. Mix ~20g Sylgard 194 PDMS as directed by the manufacturer
        - 1.4.1. Mix 18 grams of PDMS precursor with 2 grams of catalyst.
        - 1.4.2. Stir for five min
    - 1.5. Pour over silanized master in a petri dish.

1.6. Remove bubbles

1.7. Cure for 2-12 hours at 70°C

1.8. Cut PDMS off of master and segment into substrates.

1.8.1. Commonly use substrates 1 inch long by 0.5 inches wide.

2. *Load gradient precursor material.* Discontinuously dewet a high concentration of precursor material into the wells.

2.1. Place the substrate vertically into the concentrated solution (1-10 M) and withdraw at 5-10 μm/s

3. *Establish Chemical gradient*

3.1. Create spreader plate. Take a glass slide, expose to 100W oxygen plasma for 30 s, then place in a 2% solution of 600 MW polyethylene glycol for 20-30 min

3.2. Place a 0.5-2 μL droplet of distilled water on one end of the microwell substrate.

3.3. Spread droplet across the short axis of the microwell substrate with the spreader plate.

3.3.1. Use the slightly hydrophilic spreader plate to 'pull' the droplet into a line of liquid across the substrate.

3.4. 'Pull' the droplet across the substrate at 2-10 μm/s

3.4.1. This dissolves the preloaded material into the droplet, increasing the concentration of solute. As the droplet is pulled past the wells, the current concentration of material is deposited into those wells on the trailing edge, while the leading edge dissolves more material, increasing the concentration within the droplet.

4. *Characterize with SEM or AFM.*

Jeremy Barton

835 Madison St. · Evanston, IL 60202 · 847-722-7041 · *bartonj@northwestern.edu*

EDUCATION

Northwestern University, Evanston, IL
Ph.D. Candidate, Chemistry, Anticipated Graduation: May 2008
Dissertation: *Inorganic Nanowells and Nanotubes as Templates for Chemical Nanofabrication*

Grinnell College, Grinnell, IA
B.A., Biology, May 2002

HONORS AND AWARDS

- **Nanoscale Science and Engineering Center Fellow** from Northwestern University (2003-2006)
- **National Honors Scholar** at Grinnell College (1998-2002)

RESEARCH EXPERIENCE

Northwestern University, Department of Chemistry, Evanston, IL
Graduate Research Assistant, September 2002 – Present
Research Advisor: Teri W. Odom

- Developed silicon imprint lithography to generate inorganic templates for nanocrystal growth
- Discovered and optimized self-ordering anodic growth of tantalum oxide nanotubes
- Optimized tantalum oxide nanotube growth to generate 0.5 aspect ratio tubes suitable to use as large area inorganic templates for nanocrystal growth.
- Used lithographic techniques to fabricate micro and nanoscale (100-3000 nm) structures for confining and manipulating proteins to microreactors.
- Developed secondary dewetting method for establishing a gradient of concentrations across an array of surface microwells and applied to screening protein crystallization conditions.
- Helped assemble instrumentation for optical characterization of nanoscale structures.
- Helped establish a new laboratory by setting up new equipment and instrumentation.
- Demonstrated scientific instrumentation for students, teachers and professors.

Grinnell College, Department of Biology, Grinnell, IA
Undergraduate Research Assistant, January 2001 – July 2002
Research Advisor: Bruce Voyles

- Applied inverse polymerase chain reaction to isolate stationary phase genes in *acinetobacter calcoaceticus*

TEACHING EXPERIENCE

Northwestern University, School of Continuing Studies, Evanston, IL
Teaching Assistant, Fall 2006, Fall 2007, Winter 2007, Spring 2008

- Taught laboratory section in general chemistry, wrote solutions to homework assignments, and graded exams.
- Assisted students with writing and presentation skills, time management, problem solving, and critical scientific thinking.
- Held review sessions before midterms and final exam.

Northwestern University, Department of Chemistry, Evanston, IL
Teaching Assistant, Fall 2002, Fall 2003

- Taught an advanced laboratory section on MALDI-TOF mass spectrometry in senior level analytical laboratory
- Developed and optimized laboratory techniques and samples on MALDI-TOF mass spectrometry.

PUBLICATIONS

Wang, L.; Lee, M. Y.; **Barton, J.**; Hughes, L.; Odom, T. W., Shape-Control of Protein Crystals in Patterned Microwells. *J. Am. Chem. Soc.* **2008,** 130, (7), 2142-2143.

Henzie, J.; Barton, J. E.; Stender, C. L.; Odom, T. W., Large-Area Nanoscale Patterning: Chemistry Meets Fabrication. *Accounts of Chemical Research* **2006,** 39, (4), 249-257.

Greyson, E. C.; **Barton, J. E.**; Odom, T. W., Tetrahedral zinc blende tin sulfide nano- and microcrystals. *Small* **2006,** 2, (3), 368-371.

Sekar, P.; Greyson, E. C.; **Barton, J. E.**; Odom, T. W., Synthesis of Nanoscale NbSe2 Materials from Molecular Precursors. *Journal of the American Chemical Society* **2005,** 127, (7), 2054-2055.

Barton, J. E.; Odom, T. W., Mass-Limited Growth in Zeptoliter Beakers: A General Approach for the Synthesis of Nanocrystals. *Nano Letters* **2004,** 4, (8), 1525-1528.

Babayan, Y.; **Barton, J. E.**; Greyson, E. C.; Odom, T. W., Templated and hierarchical assembly of CdSe/ZnS quantum dots. *Advanced Materials* **2004,** 16, (15), 1341-1345.

SELECTED PRESENTATIONS

Barton, J.E.; Odom, T.W., Nanowells and Nanotubes by Anodization of Tantalum Oxide, Northwestern University Department of Chemistry Physical Chemistry Seminar Presentation (May 2007).

Barton, J.E.; Odom, T.W., Mass limited chemical gradients: Applications in protein crystallization, Oral presentation at the 233rd American Chemical Society National Meeting, Chicago, IL (March 2007).

Barton, J.E.; Odom, T.W., Hierarchical assembly in silicon zeptoliter beakers, Oral presentation at the 233rd American Chemical Society National Meeting, Chicago, IL (March 2007).

Barton, J.E.; Babayan, Y.; and Odom, T.W. *Nanoscale Patterning and Assembly of Nanocrystals*. Poster Session at the NSF site visit to the Nanoscale Science and Engineering Center at Northwestern University, Evanston, IL (June 2005).

Barton, J.E.; Odom, T. W., Mass-limited growth in zeptoliter beakers: A general approach for the synthesis of nanocrystals. In *229th ACS National Meeting*, San Diego, CA, United States, 2005.

Barton, J.E.; Odom, T.W. *Mass-limited growth in zeptoliter beakers: A general approach for the synthesis of nanocrystals.* Oral Presentation to the NSF site visit to the Nanoscale Science and Engineering Center at Northwestern University, Evanston, IL (June 2003)

OUTREACH ACTIVITIES

- Organized a presentation on nanotechnology for "FIRST LEGO League 2006-2007 NANO" and provided technical and scientific help to the participating students from the Chicago, IL region (October 2006).

- Participated in a science outreach program for third and fourth graders at Steven K. Hayt Elementary School, Chicago, IL. Responsibilities included writing lesson plans, leading a group of graduate student volunteers, teaching science to a group of fourth graders, and organizing an end-of-the-year science demo (January 2006 May 2007).

- Lead scientific instrumentation demonstrations for high school students, Northwestern University, Evanston, IL (2004-2007).

- Participated in the 2nd – 5th annual "Nanoscience Day" for local Boy Scout and Girl Scout troops by conducting demonstrations of advanced laboratory instrumentation, helping with hands-on lab experiments demonstrating nanoscience/technology, and presenting near term technological possibilities of nanotechnology at Northwestern University, Evanston, IL (2003-2006).

PROFESSIONAL AFFILIATIONS

- American Chemical Society (ACS)
- American Physical Society (APS)
- Materials Research Society (MRS)

- Phi Lambda Upsilon, Graduate Chemistry Honor Society

SKILLS

- **Microscopy:** light microscopy (dark field and bright field), scanning electron microscopy (SEM), transmission electron microscopy (TEM), atomic force microscopy (AFM).
- **Fabrication and Assembly:** Electron-beam lithography, photolithography, phase-shifting photolithography, imprint lithography
- **Thin Film Deposition:** Electron beam deposition, plasma-sputtering, Langmuir-Blodgett.
- **Spectroscopy:** Extensive experience with: UV-visible extinction, dark field scattering, single particle spectroscopy, fluorescence spectroscopy. Laboratory experience with: Nuclear magnetic resonance (NMR), infrared absorption (IR), mass spectrometry (MS), matrix-assisted laser desorption time of flight mass spectrometry (MALDI-TOF)
- **Synthesis:** colloidal solution and template based nanocrystal synthesis
- **Separation techniques:** Thin layer chromatography (TLC), liquid chromatography (LC), high-pressure liquid chromatography (HPLC)
- **Electrochemistry:** Cyclic voltammetry (CV), chronoamperometry, electroplating, anodization
- **Lasers:** continuous wave (gas, solid state), pulsed, ultrafast (femtosecond Ti:Sapphire and harmonic generation)
- **Computer:** Microsoft Office, Adobe Illustrator, Adobe Photoshop, C programming, HTML, 3D Studio Max, Igor Pro

BUSINESS EXPERIENCE

Thunderstorm Integrated Marketing, Denver, CO
Assistant Research Analyst, May 2001 – August 2001

Implemented a national research campaign to ascertain the comparative retail product exposure of a major national brand cheese.